



HAL
open science

P–T evolution of Precambrian eclogite in the Sveconorwegian orogen, SW Sweden

Lorraine Tual, Pavel Pitra, Charlotte Möller

► **To cite this version:**

Lorraine Tual, Pavel Pitra, Charlotte Möller. P–T evolution of Precambrian eclogite in the Sveconorwegian orogen, SW Sweden. *Journal of Metamorphic Geology*, 2017, 35 (5), pp.493-515. 10.1111/jmg.12242 . insu-01424283

HAL Id: insu-01424283

<https://insu.hal.science/insu-01424283>

Submitted on 2 Jan 2017

HAL is a multi-disciplinary open access archive for the deposit and dissemination of scientific research documents, whether they are published or not. The documents may come from teaching and research institutions in France or abroad, or from public or private research centers.

L'archive ouverte pluridisciplinaire **HAL**, est destinée au dépôt et à la diffusion de documents scientifiques de niveau recherche, publiés ou non, émanant des établissements d'enseignement et de recherche français ou étrangers, des laboratoires publics ou privés.

**P–T evolution of Precambrian eclogite in the
Sveconorwegian orogen, SW Sweden.**

Journal:	<i>Journal of Metamorphic Geology</i>
Manuscript ID	JMG-16-0005.R2
Manuscript Type:	Original Article
Date Submitted by the Author:	n/a
Complete List of Authors:	Tual, Lorraine; Lunds Universitet Institutionen for geo- och ekosystemvetenskaper, Geologiska institutionen Pitra, Pavel; Université Rennes I, Géosciences Rennes; Ceska Geologicka Sluzba, Centrum výzkumu litosféry Möller, Charlotte; Lunds Universitet Institutionen for geo- och ekosystemvetenskaper, Geologiska institutionen
Keywords:	P–T path, pseudosection, Precambrian, eclogite, Sveconorwegian

***P–T* evolution of Precambrian eclogite in the Sveconorwegian orogen, SW Sweden.**

Lorraine Tual¹, Pavel Pitra^{2,3}, Charlotte Möller¹

¹ *Geologiska institutionen, Lunds universitet, Sölvegatan 12, SE-223 62 Lund, Sweden. lorraine.tual@gmail.com*

² *Géosciences Rennes, UMR CNRS 6118, Université de Rennes 1, 35042 Rennes, Cedex, France*

³ *Česká geologická služba, Klárov 3, 118 21, Praha 1, Czech Republic*

Short title: *P–T* evolution of Precambrian eclogite, SW Sweden.

ABSTRACT

Conditions of the prograde, peak-pressure and part of the decompressional *P–T* path of two Precambrian eclogites in the eastern Sveconorwegian orogen have been determined using the pseudosection approach. Cores of garnet from a Fe-Ti-rich eclogite sample record a first prograde and syn-deformational stage along a Barrovian geothermal gradient from ~670 °C and 7 kbar to 710 °C and 8.5 kbar. Garnet rims grew during further burial to 16.5–19 kbar at ~850–900 °C, along a steep dP/dT gradient. The pseudosection model of a kyanite-bearing eclogite sample of more magnesian bulk composition confirms the peak conditions. Matrix reequilibration associated with subsequent near-isothermal decompression and partial exhumation produced plagioclase-bearing symplectites replacing kyanite and clinopyroxene and is estimated at 850–870 °C and 10–11 kbar. The validity of the pseudosections is discussed in detail. It is shown that in pseudosection modelling the fractionation of FeO in accessory sulphides may cause a significant shift of field boundaries (here displaced by up to 1.5 kbar and 70 °C) and must not be neglected.

Fast burial, exhumation and subsequent cooling are supported by the steepness of both the prograde and the decompressional *P–T* paths as well as the preservation of garnet growth zoning and the symplectitic reaction textures. These features are compatible with deep tectonic burial of the eclogite-bearing continental crust as part of the underthrusting plate (Eastern Segment, continent Baltica) in a collisional setting that led to an effectively doubled crustal thickness and subsequent exhumation of the eclogites through tectonic extrusion. Our results are in accordance with regional structural and petrologic relationships, which demonstrate foreland-vergent partial exhumation of the eclogite-bearing nappe along a basal thrust zone and support a major collisional stage at *c.* 1 Ga. We argue that the similarities between Sveconorwegian and Himalayan eclogite occurrences emphasize the modern style of Grenvillian-aged tectonics.

Keywords: *P–T* path, pseudosection, Precambrian, eclogite, Sveconorwegian.

INTRODUCTION

Pressure–temperature (*P–T*) paths of exhumed high-pressure rocks place fundamental constraints on the tectonothermal evolution of an orogen. Eclogites are markers of

collision zones, especially in the case of old orogens, which today occur as dispersed fragments over the Earth. As such, the eclogite-bearing region of SW Sweden is a critical tectonic feature of the Sveconorwegian orogen, and furthermore important for understanding of the large-scale geodynamics of the supercontinent Rodinia. However, whereas the qualitative P - T - t path of the Precambrian eclogites in SW Sweden is known (Möller, 1998, 1999), quantitative data on the prograde path and the peak P - T conditions have been lacking. The occurrences of Precambrian eclogites are few, and accurate P - T data critical for assessment of temperature and pressure regimes in Precambrian times (cf. Brown, 2014).

Eclogites in the Sveconorwegian orogen are structurally confined to a regional recumbent fold nappe in the eastern part of the orogen (Möller *et al.*, 2015), with the base of the nappe marked by a high-temperature shear zone (Tual *et al.*, 2015). The eclogites form lenses within migmatitic felsic gneisses and constitute an original part of the continental crust (e.g., Johansson *et al.*, 2001; Möller *et al.*, 2015). The general P - T path for the Sveconorwegian eclogites has been outlined by Möller (1998, 1999). The P - T conditions of reequilibration during decompression were bracketed at $\sim 770 \pm 50$ °C and 10.5 ± 2 kbar; the peak-pressure conditions were only broadly estimated at $P > 15$ kbar (Möller, 1998; Austin Hegardt *et al.*, 2005).

In this study we determine the P - T paths of two eclogite samples of different bulk composition and show that the steepness of both the prograde and retrograde paths reflect short-lived episodes of burial and exhumation. Our P - T data show burial of the continental crust to ~ 18 kbar (~ 65 km depth) at 860 °C, implying a doubled thickness of the continental crust at the end of the Sveconorwegian orogeny, and subsequent tectonic exhumation of the eclogites – a scenario similar to the Himalayas.

GEOLOGICAL SETTING

The Sveconorwegian orogen

The 1.1-0.9 Ga Sveconorwegian orogen is part of the global Grenvillian-aged orogenic belt (supercontinent Rodinia). It is composed of five crustal segments, which are separated by roughly N-S-trending crustal shear zones; from west to east these are the Telemarkia, Bamble, Kongsberg, and Idefjorden Terranes, and the Eastern Segment (Fig. 1; Bingen *et al.*, 2005; Bingen *et al.*, 2008a and references therein). A west-dipping belt of intense ductile deformation, the Mylonite Zone, separates the Idefjorden Terrane from the Eastern Segment. Four main tectono-metamorphic events have been identified (Bingen *et al.*, 2008a). The *c.* 1.14 Ga Arendal phase in the Bamble and Kongsberg Terranes involved metamorphism at granulite- and upper amphibolite-facies at intermediate pressures (Engvik *et al.*, 2016). The *c.* 1.05-1.02 Ga Agder phase is recorded in the Telemarkia and Idefjorden Terranes, as mostly greenschist- to upper amphibolite-facies metamorphism. High-pressure granulite-facies conditions have however been recorded locally in the Idefjorden Terrane just west of the Mylonite Zone (Söderlund *et al.*, 2008). In Telemarkia, a granite suite intruded at 1.05-1.02 Ga (Bingen, 1989; Bingen & van Breemen, 1998; Bingen & Solli, 2009; Slagstad *et al.*, 2012). The subsequent Falkenberg phase at 0.99-0.98 Ga caused high-pressure and high-temperature metamorphism of the southern Eastern Segment, reaching eclogite-facies conditions preserved in an eclogite-bearing nappe (Figs 1 & 2; Möller *et al.*, 2015). In the Eastern Segment, partial melting at 0.98-0.96 Ga was followed by intrusion of pegmatite and mafic dykes (e.g. Möller *et al.*, 2007, 2015). The post-collisional Dalane phase includes the intrusion of an Anorthosite-

Mangerite-Charnockite-Granite (AMCG) suite in terranes west of the Mylonite Zone, and associated high-temperature metamorphism in Telemarkia at *c.* 0.93-0.92 Ga (e.g. Vander Auwera *et al.*, 2011).

The Eastern Segment and the eclogite-bearing nappe

The bedrock east of the Sveconorwegian orogen (Fig. 1) comprises 2.0-1.8 Ga (Svecokarelian/Svecofennian) igneous and meta-igneous rocks (e.g. Stephens *et al.*, 2009; Stephens & Andersson, 2015) and rocks of the 1.86–1.66 Ga Transcandinavian Igneous Belt (TIB). These rocks can be followed westwards into the Eastern Segment where they become increasingly deformed. Most of the Eastern Segment is made up of *c.* 1.7 Ga orthogneisses equivalent to the TIB intrusions (e.g. Wahlgren *et al.*, 1994; Söderlund *et al.*, 1999, 2002; Andersson *et al.*, 2002; Möller *et al.*, 2007, 2015; Petersson *et al.*, 2015). The eastern limit of Sveconorwegian ductile deformation is marked as the Sveconorwegian Front in Fig. 1.

A 50 x 75 km large eclogite-bearing fold nappe is situated in the internal section of the Eastern Segment, at the contact with the overlying Idefjorden Terrane (Figs 1 & 2; Möller *et al.*, 2015). Rocks enclosing this nappe are upper amphibolite- and high-pressure granulite-facies gneisses (Johansson *et al.*, 1991; Wang & Lindh, 1996), which are in most places migmatitic and show penetrative deformation and polyphasal folding (Andersson *et al.*, 1999, 2002; Söderlund *et al.*, 2002; Möller *et al.*, 2007, 2015; Hansen *et al.*, 2015; Piñán-Llamas *et al.*, 2015). The contact of the nappe with the surrounding orthogneisses is marked by semi-continuous 1.4 Ga augen orthogneiss (Fig. 2; Möller *et al.*, 2015).

Eclogite occurs as lenses in stromatic migmatite gneisses within the fold nappe, and in the basal high-temperature shear zone (Fig. 2; Möller, 1998, 1999; Austin Hegardt *et al.*, 2005; Möller *et al.*, 2015; Tual *et al.*, 2015). Orthogneisses within the eclogite-bearing nappe have been dated at 1.74-1.66 Ga, demonstrating that the nappe is indigenous to the Eastern Segment (Möller *et al.*, 2015). The nappe represents a part of the continental crust that experienced westward tectonic burial at eclogite-facies conditions beneath the Idefjorden Terrane, and was followed by eastward, foreland-directed, tectonic exhumation (Möller *et al.*, 2015). The eclogites were part of the Baltica continental crust prior to the onset of the Sveconorwegian orogeny and consequently do not represent a detached piece of an oceanic slab (Johansson *et al.*, 2001; Möller *et al.*, 2015).

The high-temperature tectonites from the basal thrust zone testify to tectonic exhumation of the eclogite-bearing nappe and stalling at a mid-crustal orogenic level at ~10 kbar (~40 km; Möller *et al.*, 2015; Tual *et al.*, 2015). Syn-deformational leucosome indicate that nappe emplacement was aided by the presence of melt. The prograde metamorphism leading to eclogitization was first dated at 972 ± 14 Ma (SIMS U-Pb on zircon; Johansson *et al.*, 2001) and recently refined at 988 ± 6 Ma (SIMS U-Pb on zircon; Möller *et al.*, 2015). The crystallization of leucosome has been bracketed between 976 ± 6 Ma and 956 ± 7 Ma (i.e. starting after eclogitization, Möller *et al.*, 2015).

Various types of eclogite are present in the nappe. The field relations, petrology and structural geology of the eclogites and their country rocks have been documented in detail in Möller (1998, 1999), Austin Hegardt *et al.* (2005), Möller *et al.* (2015), and Tual *et al.* (2015). The samples studied in this paper were taken from mafic bodies in the basal shear zone (Fig. 2), and represent rare varieties, with limited retrogression, of Fe-Ti-rich eclogite (sample MU6) and kyanite-bearing eclogite (sample 8023F).

METHODS

Mineral X-ray maps and analyses were performed using a JEOL JXA-8200 Superprobe, fitted with five wavelength dispersive spectrometers (WDS) and an energy dispersive spectrometer (EDS) at the University of Copenhagen. The analytical conditions were set at 15.0 kV acceleration voltage and 15 nA probe current. Standards were natural albite (Na), orthoclase (K), corundum (Al), wollastonite (Ca, Si), forsterite (Mg), hematite (Fe), pyrophanite (Mn), chromite (Cr), apatite (F) and synthetic rutile (Ti). Complementary analyses and imaging were made using a Hitachi 3400N scanning electron microscope equipped with an Oxford EDS. Bulk rock compositions and FeO (vs. Fe₂O₃) were analysed in ACME Vancouver (Canada), from powders prepared at the Lund University using a tungsten-carbide mill.

Mineral abbreviations are those used by THERMOCALC (Holland & Powell, 2011). Pseudosections were calculated using THERMOCALC 3.4 (Powell *et al.*, 1998) and the dataset ds55 (updated Nov. 2003; Holland & Powell, 1998) in the system NCKFMASHTO (Na₂O–CaO–K₂O–FeO–MgO–Al₂O₃–SiO₂–H₂O–TiO₂–O). Mixing models for solid solutions were taken from Diener *et al.* (2007; amphibole, clinopyroxene), White *et al.* (2007; garnet, biotite), Holland *et al.* (1998; chlorite), Coggon & Holland (2002; paragonite, muscovite), Holland & Powell (2003; plagioclase, K-feldspar), White *et al.* (2002; magnetite, spinel), Holland & Powell (1998; talc, epidote), White *et al.* (2000; hematite, ilmenite). Epidote was modeled as a solid solution rather than the pure end-member (clino)zoisite, to account for the small amount of Fe³⁺ in the analysed crystals. In the phase diagrams, the term hornblende (hb) is used *sensu lato* (cf. Dale *et al.*, 2005) rather than in the strict sense of Leake *et al.* (1997). Mineral proportions are estimated through image analysis of the thin sections (pseudo-colouring of minerals and pixel ratio determined using Photoshop).

Mineral compositions are given in mole % unless stated otherwise. Cpfu = cations per formula unit. $X_{Fe} = Fe^{2+}/(Fe^{2+}+Mg)$; $An = 100 \times Ca/(Ca+Na+K)$; $Jd = 100 \times Na \text{ cpfu}$; $Prp = 100 \times Mg/(Ca+Fe^{2+}+Mg+Mn)$; $Alm = 100 \times Fe^{2+}/(Ca+Fe^{2+}+Mg+Mn)$; $Sps = 100 \times Mn/(Ca+Fe^{2+}+Mg+Mn)$. In pseudosections, the mole fraction of grossular is defined as $z(g) = (Ca/(Ca+Fe^{2+}+Mg)) \times 100$, because a Mn-free model system is used. However, for the sake of simplicity, and given the low proportion of spessartine in garnet (see below), modelled $z(g)$ is considered equivalent to measured $Grs = 100 \times Ca/(Ca+Fe^{2+}+Mg+Mn)$. The symbol “→” is used to describe the compositional change from core to rim.

PETROGRAPHY AND MINERAL CHEMISTRY

Two samples of different bulk rock composition were selected for a detailed petrological analysis: Fe-Ti-rich quartz-bearing eclogite and Mg-Al-rich kyanite-bearing eclogite (Fig. 3a, b). Textures and mineral compositions, including detailed zoning patterns, of these rock types are documented in Möller (1998, 1999); here we focus on the two samples that were selected for thermodynamic modelling. Table 1 shows representative analyses of minerals; Table 2 shows whole-rock compositions of the two samples in wt. %.

Fe-Ti eclogite (sample MU6)

Sample MU6 represents a Fe-Ti-rich layer from a 2.5 x 1.5 km large eclogite-bearing mafic body (Fig. 2; WGS84: 57°09'21.3"N 12°42'49.4"E, locality: Ammås). The investigated thin section is made up of garnet (~60 vol.%) + quartz (~20 vol.%) + clinopyroxene (~10 vol.%) + rutile (~3 vol.%; Fig. 3a), associated locally with variable amount of amphibole and plagioclase. Accessory minerals include apatite, zircon and ilmenite.

Garnet generally has a distinct core-and-rim structure. Elongated inclusions in the core define straight, gently bent or locally sigmoidal trails, and comprise rutile, quartz, plagioclase, apatite and locally amphibole (Fig. 4). A nearly inclusion-free outer core separates the inclusion-rich core from the rim, where rutile, quartz and apatite grains are 5-10 times larger and unoriented or their orientation follows the garnet rim (Fig. 4c-e). A smooth rimward decrease of almandine, spessartine, and X_{Fe} ($Alm_{55} \rightarrow 46$, $Sps_3 \rightarrow 1$, $X_{\text{Fe}} 0.76 \rightarrow 0.61$) is balanced by a smooth increase of pyrope ($Prp_{17} \rightarrow 32$). There is a slight zoning of grossular: an increase ($Grs_{24} \rightarrow 27$) in the inclusion-rich garnet core, constant or only slight increase in the inclusion-free outer core (Grs_{27-28}), and a decrease in the rim ($Grs_{28} \rightarrow 25$). A final decrease in the outermost rim is also common ($Grs_{26} \rightarrow 24$; Fig. 4b-e; Table 1a) usually associated with a slight increase in pyrope (28 \rightarrow 30; Fig. 4e, see also Möller, 1998). The right side of the garnet profile in Fig. 4b shows a drop in grossular associated with a slight decrease in almandine and increase in pyrope that is likely due to local reequilibration around a crack.

Clinopyroxene crystals are generally 2-10 mm large. They commonly contain inclusions of amphibole, quartz and plagioclase (the latter forming up to 50 vol.% of the clinopyroxene poikiloblast; Fig. 5a) and have the composition of diopside with low jadeite content ($X_{\text{Fe}} = 0.10-0.22$, clustering around 0.18-0.20, Jd_{2-10} , $Al = 0.05-0.32$ cpfu; Fig. 5a; Table 1a). Area analyses (covering ~2 x 1 mm) of diopside + plagioclase give, however, values of $X_{\text{Fe}} \approx 0.29$ and Jd_{18} . Clinopyroxene inclusions in garnet rims are more magnesian ($X_{\text{Fe}} = 0.10-0.13$). The Ca-Tschermak component ranges between 0 and 10% regardless of textural position (Table 1a). Clinopyroxene is locally partly replaced by amphibole (Fig. 5b).

Amphibole occurs as inclusions in garnet cores (Fig. 5c), but also as partial replacements of clinopyroxene in the matrix (Fig. 5b). The composition corresponds in general to hornblende, although some inclusions in garnet classify as pargasite or tschermakite (Fig. 5d). X_{Fe} is generally close to 0.30 but is up to 0.73 in grains included in garnet; $X_{\text{Na}_{M4}} = [Na/(Na+Ca)]_{M4} = 0.03-0.04$ (Fig. 5d); $K = 0.01-0.09$ cpfu but generally around 0.03; recalculated Fe^{3+} ranges between 0.12 and 0.31 cpfu; $Ti = 0.14-0.28$ cpfu (Table 1b).

Plagioclase occurs as inclusions in the garnet core (Fig. 5e) and in clinopyroxene (up to 50 vol.%; Fig. 5a). The composition of the inclusions in clinopyroxene is An_{45-55} (Fig. 5a,f), inclusions in garnet core vary strongly from An_{40} to An_{81} (Fig. 5f).

Quartz forms large grains (up to 3 mm) that constitute up to 30 vol.% of the matrix (Figs 3a & 5b, g). It also occurs as oriented inclusions together with rutile in the

garnet core (0.01-0.1 mm wide; e.g. Fig. 5e) and unoriented crystals in the rim (0.05-0.30 mm).

Rutile occurs as inclusions in garnet, quartz and clinopyroxene (Figs 3a, 4a & 5b, c, e, g & h) and as a relatively abundant matrix phase (Figs 3a, 4a & 5b, g & h). A few rutile grains included in the garnet core are associated with ilmenite. The grain size of rutile increases progressively, from a few μm in the garnet cores, up to a few hundred μm in garnet rims (Fig. 5g), and up to 2 mm in the matrix (Fig. 5h). Matrix rutile is in general partly replaced by ilmenite (Figs 3a & 5h).

Kyanite eclogite (8023F)

Sample 8023F represents a layer of kyanite-bearing eclogite in an eclogite body of unknown size (Fig. 2; WGS84: 57°9'9.99"N 12°46'8.91"E; locality: Tranabo). The sample is composed of a former HP assemblage (cf. Möller, 1998) garnet (~24 vol.%), clinopyroxene (~50 vol.%), kyanite (~10 vol.%), amphibole (~12 vol.%) and locally quartz, rutile, biotite, plagioclase and sulphides (pyrite, chalcopyrite; Fig. 3b). Kyanite is in most places partly replaced and surrounded by sapphirine-plagioclase symplectite, locally containing corundum and rare spinel.

Garnet crystals are 3-8 mm in diameter and contain unoriented inclusions of kyanite, zoisite, biotite, clinopyroxene, quartz and minor apatite (Figs 3b & 6a). They are commonly anhedral and locally partly surrounded by amphibole + plagioclase symplectites (Fig. 6a, c & e). There is a rimward decrease of almandine, spessartine, and X_{Fe} ($Alm40 \rightarrow 29$, $Sps4 \rightarrow 1$, $X_{\text{Fe}} = 0.54 \rightarrow 0.37$), which is balanced by an increase of pyrope ($Prp35 \rightarrow 48$). Grossular zoning is weak: there is a progressive increase in the core ($Grs21 \rightarrow 24$), a decrease in the inner rim ($Grs24 \rightarrow 21$), followed by an increase toward the outer rim ($Grs0.23$), and locally a final *Grs* drop in the outermost rim ($Grs0.21$); Fig. 6b-e; Table 1c).

Clinopyroxene crystals (up to 8 mm) contain inclusions of plagioclase \pm amphibole and quartz, commonly elongated along crystallographic planes (Fig. 7). In the inner, inclusion-poor, part the jadeite content (*Jd*) is 18-22 and X_{Fe} 0.06-0.09. In plagioclase inclusion-rich rims *Jd* decreases to 3-5 and most X_{Fe} values are between 0.09 and 0.11 (Fig. 7; Table 1c). Inclusions of clinopyroxene in garnet have *Jd* 9-12 and X_{Fe} 0.10-0.16 (Table 1c).

Kyanite is preserved as inclusions in garnet cores, and in the matrix (0.6 mm long) in cores of plagioclase + sapphirine \pm corundum symplectites (Figs 6a & 8a, b). The symplectite domains have locally a rectangular shape and are interpreted as pseudomorphs after kyanite crystals, the initial length of which have been up to 7 mm (see also Möller 1998, 1999).

(*Clino*)zoisite/epidote is only found as inclusions in garnet cores, as up to 0.3 mm large grains, locally in direct contact with kyanite (Fig. 6a). It does not contain significant amounts of Ti or Cr, and the pistacite (epidote *sensu stricto*) content [$X_{\text{Fe}^{3+}} = \text{Fe}^{3+}/(\text{Fe}^{3+} + \text{Al}-2)$] is ~0.12 (Table 1d).

Plagioclase is present in a variety of textural settings (Figs 9a & 10a, b) and the composition varies accordingly (Figs 9a & 10b; Table 1d). *An* ranges from 91 (in symplectites with sapphirine) to 41 (intergrown with symplectitic orthopyroxene

along clinopyroxene rims). The An of inclusions in clinopyroxene ranges from 39 to 45 (Figs 9a, 10a & 10b).

Amphibole forms inclusions ($\sim 100\mu\text{m}$) in garnet and clinopyroxene, and subhedral crystals in the matrix (up to 8 mm). Associated with plagioclase, smaller crystals ($\times 100\mu\text{m}$) also commonly form coronae or rims between clinopyroxene and garnet (Figs 3b, 6a & 10a), and locally between clinopyroxene and sapphirine symplectites (Fig. 10a). Inclusions and large matrix crystals tend to be bluish-green, whereas amphibole in reaction rims tends to be of a brownish-green colour and significantly smaller. Amphibole is pargasite to edenite regardless of the textural setting: $(\text{Na}+\text{K})_A$ varies between 0.5 to 0.8 and Si varies from 6 to 6.7 cpfu (Fig. 9b; Table 1d). X_{Fe} varies between 0.12 and 0.16; $X_{\text{Na}_{M4}} < 0.1$; recalculated Fe^{3+} ranges between 0.10 and 0.30 cpfu; K clusters between 0.12 and 0.16 cpfu; Ti = 0.03-0.30 cpfu (Fig. 9b; Table 1d).

Sulphides form up to 2 vol.% of the rock and mostly comprise chalcopyrite partly replaced by covellite + goethite, and locally pyrite. Sulphide grains are commonly found in the cores of the large subhedral amphibole crystals.

Orthopyroxene forms symplectitic intergrowths with plagioclase, up to 300 μm wide, along the rims of clinopyroxene (Fig. 10a, b). One inclusion ($\sim 0.3 \times 0.1 \text{ mm}$) in garnet made of plagioclase + orthopyroxene + quartz is interpreted as the replacement product of a former inclusion of clinopyroxene (Fig. 10c). X_{Fe} varies from 0.18 to 0.30 (Table 1d). Al content varies from 0.05 to 0.09, but is generally around 0.07.

Sapphirine is intergrown with plagioclase within symplectites after kyanite (Figs 8a, b & 10a). Individual grains are up to 0.3 mm wide, but generally $\sim 10 \times 100 \mu\text{m}$ or smaller. $X_{\text{Fe}} = 0.10\text{-}0.14$ (Table 1d).

Corundum is situated in the symplectite domains after kyanite, generally forming intergrowths of acicular crystals in plagioclase (Fig. 8b). Traces of Cr and Fe are common but < 0.01 cpfu. In the center of one symplectitic micro-domain after kyanite, blocky corundum grains occur together with rutile and spinel; these grains are likely former inclusions in kyanite.

Spinel is only found locally in symplectite domains after kyanite, exclusively in contact with rutile. $X_{\text{Fe}} = 0.45$, Mn and Ti = 0, Cr ~ 0.1 cpfu.

TEXTURAL INTERPRETATION

Before interpreting the rocks using phase diagrams, the textures and variations in mineral chemistry can be summarized as follows (cf. also Möller, 1998, 1999), in the framework of three main stages can represent the metamorphic evolution of both samples presented here:

- (1) a prograde stage, M1, best defined in the Fe-Ti eclogite sample, starting with the garnet inner core growth associated with the inclusion assemblage and followed by an inclusion-free outer core domain;
- (2) a high-pressure stage, M2 corresponding in both samples to the garnet rim, omphacitic clinopyroxene, rutile, with or without amphibole, quartz and kyanite;

(3) a decompression stage, M3, defined as replacement textures on former high-pressure minerals.

Fe-Ti eclogite (sample MU6)

Garnet + quartz + clinopyroxene + rutile represent the dominant assemblage of this eclogite, probably close to the metamorphic pressure peak (M2). Inclusions in the inner core of garnet, i.e. plagioclase, amphibole, quartz and rutile, were part of a prograde metamorphic assemblage (M1) and have a sigmoidal inclusion pattern, which testifies to garnet growth during deformation. The regular rimward decrease of spessartine and X_{Fe} represents a growth zoning formed during prograde metamorphism. The numerous regularly distributed plagioclase inclusions in clinopyroxene are inferred to be late products from an originally more sodic (i.e. omphacitic) pyroxene. Ilmenite replacing matrix rutile, and amphibole replacing matrix clinopyroxene, are interpreted as secondary, lower-pressure features (M3). Chlorite and sericite are late phases that are present only very locally and probably formed by small-scale local fluid infiltration at low temperature.

Kyanite eclogite (8023F)

Large matrix crystals of clinopyroxene and subhedral amphibole are interpreted to have crystallized in equilibrium with garnet and constitute to the dominant eclogite-facies mineral assemblage (M2) together with kyanite, quartz and rutile. The rimward increase of jadeite component in clinopyroxene can be attributed to the growth along an up-pressure prograde P - T path (M1). Similarly, the regular rimward decrease of spessartine and X_{Fe} in garnet reflect growth during the M1 prograde metamorphism. Inclusions in the garnet core suggest that kyanite and zoisite were part of the primary mineral assemblage (M1) together with clinopyroxene, quartz, rutile, and minor biotite. The bluish-green amphibole crystals in the matrix are interpreted to have crystallized in equilibrium with clinopyroxene, whereas amphibole grains in reaction rims have formed late (M3), at the expense of clinopyroxene. Möller (1999) noted that large amphibole grains are Cl-bearing, similarly to amphibole grains included in garnet. Zoisite is present only as inclusions in garnet cores, whereas quartz inclusions are present even in the outermost rim. The numerous inclusions of plagioclase in some low-jadeite clinopyroxene rims are interpreted as the consequence of decompression-related plagioclase expulsion from a former omphacitic pyroxene. Orthopyroxene, sapphirine, and corundum are exclusively located within symplectitic coronae after omphacite and kyanite and are interpreted as reaction products related to decompression (M3).

P - T CONDITIONS

P - T pseudosections have been calculated in the framework (chemical system, mixing models etc.) described above, and are presented in Figs 11 & 12. The bulk rock compositions of the two samples (Table 2) were converted to mol.% and adapted to the model system (P_2O_5 was removed as apatite and MnO as spessartine).

In the absence of an appropriate melt model for metabasic systems at high pressures, the assemblages on the high-temperature side of the pseudosections may be metastable with respect to assemblages involving melt, or at least coexist with melt. However, experimental work, calculations and natural observations suggest that the topology of the phase relationships is similar when mineral assemblages coexist with fluid or melt and that the field boundaries may not move significantly (e.g. Wolf & Wyllie, 1994; Vielzeuf & Schmidt, 2001; Pattison, 2003). Moreover, the two

modelled rocks are not of typical basaltic compositions (Table 2), and presence of melt was not observed in the sampled rocks. In both rocks, biotite is stable, in very low modal proportions (< 0.5 mol.%), throughout the modelled P - T conditions (with the exception of the HP-LT and LP-HT corners); biotite is scarce or absent in our samples. This is the consequence of including K (potassium) in the chemical model system. In nature, K is taken in small quantities in amphibole (cf. Table 1b), but this is not accounted for in the mixing models used (but see Green *et al.*, 2016 for a new amphibole model).

Pseudosection for Fe-Ti eclogite (MU6)

The first recorded metamorphic stage, the prograde stage M1, corresponds to the assemblage $g + hb + pl + q + ru + ilm$ that is preserved as inclusions in the inner core of garnet. In the pseudosection, this assemblage is located at 620-820 °C, 6-9 kbar (Fig. 11a). The dominant peak assemblage $g + di + q + ru$ corresponds to the metamorphic stage M2 and is stable at pressures higher than 15 kbar. This suggests that the sample preserves a prograde P - T evolution involving a pressure increase and peak in the eclogite facies. However, the preserved garnet zoning and the chemical composition of the phases bring further constraints to this first order information.

Garnet core: The isopleths corresponding to the composition of the onset of garnet growth ($X_{Fe}0.76$, $Grs24$) intersect in the low-temperature part of the $g + hb + pl + q + ru + ilm$ field (Fig. 11b) and suggest conditions of ~675 °C at 7-7.5 kbar for the first metamorphic stage (ellipse 1a, Fig. 11a). The observed decrease in X_{Fe} and increase of Grs in the inclusion-rich garnet core (reaching $X_{Fe}0.72$, $Grs27$) suggest a (syndeformational) prograde evolution to 700-715 °C at 8-8.5 kbar (ellipse 1b, Fig. 11a). Further decrease in X_{Fe} (0.72→0.69) associated with a rather constant grossular content ($Grs27$ -28) in the inclusion-free garnet outer core is compatible with continuous garnet growth along a prograde path to 10-11 kbar, 750 °C (ellipse 1c, Fig. 11b). This part of the path is mostly located in the $g + hb + q + ru$ field and a nearly constant value of grossular of ~28 mol.% (Fig. 11b). The absence of plagioclase inclusions in the inner rim and beyond is compatible with the absence of plagioclase in this field. The prograde P - T path from 1c to 2 in Fig. 11a predicts a continuous decrease of X_{Fe} in garnet and decreasing Grs ($X_{Fe}0.67$ →0.61; $Grs28$ →25 mol.%). This isopleth pattern is in very good agreement with the observed garnet zoning and supports the robustness of the modelled P - T path.

Garnet rim: The composition of garnet ($X_{Fe}0.61$ -0.62, $Grs26$) varies little across the relatively large field $g + di + q + ru$ which correspond to the matrix assemblage and the peak-pressure metamorphic stage M2. Consequently, the analysed composition of the outer rim of garnet ($X_{Fe}0.61$, $Grs25$ -26), although in good agreement with the model, does not give strong constraints on the P - T conditions. However, the X_{Fe} isopleth for garnet (0.61) is situated above 875 °C and 16 kbar and helps targeting the conditions of the peak-pressure stage (Fig. 11b).

The composition of clinopyroxene modelled in the peak field $g + di + q + ru$ (Jd ~28, X_{Fe} ~0.18-0.24; Fig. 11c), in particular regarding the Jd content, does not fit very well with the analysed one (Jd 2-10, X_{Fe} ~0.18-0.22). This is due to late reequilibration (expelled plagioclase) — the initial clinopyroxene composition was significantly richer in jadeite. The reintegrated compositions from area analyses of clinopyroxene (Jd 15-19, $X_{Fe}0.29$) are still low in Jd , and high in X_{Fe} . These values may be far from

accurate, because of the imprecise reintegration method. Moreover, the Ca-Tschermak component in clinopyroxene (up to 10% in the analysed crystals), which is not taken into account in the mixing model used, is likely a source of discrepancy. Consequently, absolute analysed values are not used, but indicate that the clinopyroxene compositions modelled in the peak field $g + di + q + ru$ ($Jd \sim 28$, $X_{Fe} \sim 0.18-0.24$; Fig. 11c) are plausible. The peak stage is therefore restricted in the field $g + di + q + ru$ and the large ellipse 2 (Fig 11a, b) indicates a minimum pressure at the garnet isopleth X_{Fe} 0.61 at $\sim 15.5-19$ kbar, $850-900$ °C.

Plagioclase, amphibole, ilmenite, and the clinopyroxene-plagioclase intergrowths are interpreted as reaction products of post-peak partial reequilibration and correspond to the metamorphic stage M3. These textures are classic decompression and cooling features in eclogites. In the framework of the calculated pseudosection the stabilization of plagioclase, and in particular the expulsion of plagioclase from omphacitic clinopyroxene, is compatible with decompression from the peak peak pressure (ellipse 2, Fig. 11a) to lower pressures in the plagioclase-bearing field $g + di + pl + q + ru$ (12-16 kbar, >825 °C). The modelled composition of plagioclase along the path from ellipse 2 to 3 (Fig. 11a; $An_{0.35-0.55}$; in Fig. 11c) agrees with that of the expelled plagioclase grains in clinopyroxene (An_{45-55}). Further decompression below ~ 12 kbar to the field $g + di + hb + pl + q + ru + ilm$ (810-870 °C, 8-12 kbar) accounts for the partial replacement of rutile by ilmenite and the crystallization of amphibole at the expense of clinopyroxene (ellipse 3; Fig. 11a).

Pseudosection for kyanite-eclogite (8023F)

The prograde M1 metamorphic assemblage $g + di + hb + ky + ep + q + ru$, preserved as inclusions in the garnet cores, is stable within a narrow trivariant field (highlighted in yellow, Fig. 12a) located from 710 °C at 18 kbar to 830 °C at 15 kbar. The main matrix assemblage, representing the peak assemblage M2, corresponds to the epidote-absent field $g + di + hb + ky + q + ru$, at higher temperature and pressure than the M1 assemblage. The local presence of quartz in the matrix and as inclusions in garnet rims suggests that the P - T evolution did not go significantly beyond the quartz-out line at ~ 18 kbar.

In the pseudosection, the X_{Fe} values of garnet decrease regularly with increasing pressure and temperature (Fig. 12b). In contrast, the grossular isopleths have a maximum centered around the $g + di + hb + pl + ep + q + ru$ field and the small $g + di + hb + pl + ky + ep + q + ru$ field ($\sim 770-850$ °C, $\sim 11-15$ kbar), extending this maximum towards LT and HP , broadly along the yellow high-lighted $g + di + hb + ky + ep + q + ru$ field. Accordingly, the analysed X_{Fe} decrease in the garnet core (0.54 \rightarrow 0.45) is compatible with a progressive garnet growth during the M1 prograde stage from 13.5 kbar / 800 °C (ellipse 1) to the adjacent kyanite-bearing field corresponding to the assemblage included in garnet cores (Fig. 12a, highlighted yellow field). Further decrease of the analysed X_{Fe} ratio from garnet inner to outer rim (0.45 \rightarrow 0.37) is compatible with garnet growth during a continuous P and T increase towards the high-pressure part of the M2 field ($g + di + hb + ky + q + ru$; Fig. 12b, large yellow ellipse). Such a P - T path, passing through the “grossular high” in the pseudosection, is qualitatively compatible with the analysed garnet zoning (an increase followed by a decrease: $Grs_{21}\rightarrow 24\rightarrow 21$). However, the modelled values are significantly higher (Grs_{25-40}) than the measured ones and cannot be used to constrain the P - T path.

The analysed composition of the large matrix clinopyroxene (*Jd9-24*, clustering around 20-22, $X_{\text{Fe}} \sim 0.08$) is compatible with values modelled in the M2 field $g + di + hb + ky + ru \pm q$ (Fig. 12c, green ellipse). The best fit between observations and model (assemblage and mineral compositions) is reached for both garnet and clinopyroxene at 840-890 °C, 16.5-18 kbar (ellipse 2; Fig. 12a).

In order to verify the robustness of the P - T estimates for the peak M2 stage, modal proportions of the minerals were modelled (Fig. 13) and compared with observations. The amounts of minerals corresponding to the M2 stage were inferred from the textures in the thin section (i.e., volumes of sapphirine-plagioclase symplectite correspond to M2 kyanite, plagioclase+ clinopyroxene intergrowths correspond to M2 omphacite). The former amount of garnet (~24 vol.%), clinopyroxene (~50 vol.%), amphibole (~12 vol.%) and kyanite (~10 vol.%) are shown as dashed areas in Fig. 13. The intersection of these areas is in excellent agreement with the position of ellipse 2 in Fig. 12 (deduced from mineral compositional data) and constitutes a strong constraint of the M2 peak at 860-900 °C, 16.5-18 kbar.

The development of plagioclase-bearing symplectites, corresponding to stage M3, reflects the rock entering plagioclase-bearing fields due to decompression (dashed line in Fig. 12a), also leading to a decrease in the modal proportion of garnet and kyanite. The variable symplectitic textures associated with a strong chemical zoning suggest that they reflect conditions with inefficient diffusion, dominated by micro-scale local equilibria and different micro-scale chemical domains rather than homogeneous reequilibration (cf. Möller, 1998, 1999; Pitra *et al.*, 2010). Consequently, they cannot be quantitatively interpreted in a pseudosection calculated for the whole-rock bulk composition.

In summary, the two samples share the same P - T path, but the tightness of the P - T constraints differ between the two samples. The garnet zoning and inclusions of the Fe-Ti-rich eclogite sample allowed to recover details of the prograde evolution (M1), starting at ~670-700 °C at 7-7.5 kbar and progressing to 10-11 kbar at 750 °C. The tightest constraints, 860-900 °C, 16.5-18 kbar, of the metamorphic pressure peak (M2) were retrieved from the mineral modes of the kyanite-eclogite sample, although the same conditions (less tightly constrained) were inferred from the mineral compositions in both samples. The decompressional stage M3 corresponds to a decompression from the M2 peak to 815-870 °C, 8-12 kbar and involves local-scale equilibria only, but is possibly more accurately recorded in the pseudosection of the Fe-Ti-rich eclogite sample than in that of the kyanite eclogite.

DISCUSSION

Validity of the pseudosections

Pseudosections are phase diagrams calculated for a specific bulk composition. The estimation of this composition is subject to different sort of uncertainties and presumptions that merit a brief discussion. Pseudosections may be particularly sensitive to variations of the bulk X_{Fe} ($[\text{Fe}/(\text{Fe}+\text{Mg})]$) ratio, e.g. Powell & Holland, 1990; White *et al.*, 2001) as well as the amount of available H_2O (e.g. Guiraud *et al.*, 1996; Carson *et al.*, 1999; López-Carmona *et al.*, 2013).

Fe content in sulphides and consequences

Fe-sulphides are common, albeit accessory, constituents of silicate, in particular metabasic, rocks. However, their influence on the bulk X_{Fe} ratio is rarely discussed. In the kyanite-eclogite (8023F) they are interpreted as part of the initial to early prograde metamorphic assemblage and do not appear to participate in reaction textures, apart from late-stage reequilibrations (chalcopyrite transformation to covellite and goethite). Although they only form around 2 vol.% of the thin section (estimated by point counting), they can fractionate a non-negligible amount of ferrous iron from the bulk composition. Therefore, a pseudosection for the kyanite-eclogite was calculated to test the effect of neglecting the iron fractionation in sulphides (Fig. 14a, b). In this case, it results in a modification of the bulk X_{Fe} ratio from 22 to 26 and causes a significant shift of the garnet- and kyanite-in lines of up to 1.5 kbar and 70 °C towards high-pressure and temperature (Fig. 14b). The clinopyroxene-in line is shifted by ~25 °C to higher temperatures; as a consequence, the size of the central field (g + hb + ep + q + ru) is smaller. However, the field corresponding to the peak assemblage is broadly similar in both cases (i.e. with or without of iron fractionation). The grossular isopleths are only little affected, but X_{Fe} isopleths are significantly displaced to lower P and T by up to 1.5 kbar and 20 °C, resulting in a poorer agreement between calculations and observations (Fig. S1). Clearly, taking the Fe fractionation in sulphides into account must not be neglected, even if they are present in apparently low proportions. Pseudosections including a full set of isopleths and P/T - $X(\text{H}_2\text{O})$ and $-X(\text{Fe}_2\text{O}_3)$ content are provided in Figs. S1 & S2 for comparison.

Fe₂O₃ content

Beyond the effect of the Fe^{2+} fractionation in sulphides, bulk X_{Fe} is strongly influenced by the estimation of the amount of ferric iron. Although the analytical determination of the Fe^{3+} is common practice, López-Carmona *et al.* (2013) have shown that the proportion of Fe^{3+} can be easily modified by superficial alteration even in apparently fresh samples, and argued for a systematic use of P/T - $X(\text{Fe}_2\text{O}_3)$ pseudosections [$X(\text{Fe}_2\text{O}_3) = 2\text{Fe}_2\text{O}_3 / (2\text{Fe}_2\text{O}_3 + \text{FeO}) = \text{Fe}^{3+} / (\text{Fe}^{3+} + \text{Fe}^{2+})$]. In both samples studied, the amount of Fe^{3+} vs. Fe^{2+} was analysed (FeO by titration) and these values were used for calculating the pseudosections presented above.

For the Fe-Ti-rich eclogite, a P - $X(\text{Fe}_2\text{O}_3)$ pseudosection was calculated to test the effect of Fe_2O_3 on the predicted assemblages and compositions, at 760 °C and from 8 to 18 kbar (Fig. 15). The analysed Fe_2O_3 content corresponds to $X(\text{Fe}_2\text{O}_3) = 0.09$. The assemblages do not substantially change from $X(\text{Fe}_2\text{O}_3) = 0$ to 0.09, therefore adjusting the Fe_2O_3 content to values lower than the one analysed is unjustified. Slightly higher values of Fe_2O_3 result in the appearance of ilmenite up to 18 kbar and the stabilization of epidote, which is incompatible with the observations. Consequently, using the analysed Fe_2O_3 content in the sample appears as the best option for the Fe-Ti-eclogite.

For the kyanite-eclogite, the main issue is the modelled high grossular content in garnet cores, which does not fit the analysed composition. Therefore, the calculations aimed particularly at investigation of the influence of the Fe_2O_3 variation on the position of the garnet isopleths. In the P - $X(\text{Fe}_2\text{O}_3)$ pseudosection calculated at 800 °C (Fig. 16), the increase of the Fe_2O_3 content leads very abruptly to diopside not being stable, whereas it is found as inclusion in garnet. Although both increasing or decreasing $X(\text{Fe}_2\text{O}_3)$ leads to lowering the modelled Grs values, those observed in the garnet cores (Grs21→24) are never reached. Furthermore, the increase of the Fe_2O_3 content leads very abruptly to diopside not being stable in the assemblage, and the decrease of Fe_2O_3 leads to the disappearance of epidote, whereas both minerals are

present as inclusions in garnet. Consequently, values of Fe_2O_3 significantly different from the analyzed one produce an even poorer agreement between the model and the observations. A similar effect is observed in pseudosections, where the fractionation of Fe^{2+} in sulphides was not taken into account – the variation of Fe_2O_3 does not provide better results (Fig. S2). Consequently, the analysed amount of Fe_2O_3 was used.

H₂O content

Because of the dehydration character of a vast majority of metamorphic reactions (along a prograde evolution), most rocks are saturated in H_2O , which is then commonly considered in excess. Whereas this approach usually yields correct results, and is generally a good starting point, care is needed in some cases. These include rocks undergoing partial melting (e.g. Powell, 1983; White *et al.*, 2001), subduction-related metamorphism (e.g. Ballèvre *et al.* 2003; López-Carmona *et al.*, 2013), retrograde evolution (e.g. Guiraud *et al.*, 2001; Pitra *et al.*, 2010), and also the metamorphism of H_2O -poor protoliths. This is the case of rocks that have been previously dehydrated (polycyclic metamorphic rocks), but also unaltered magmatic rocks (granites, gabbros, dolerite dykes, etc.), and the studied samples may belong to one of the latter cases.

Although the H_2O -saturated pseudosection for the Fe-Ti eclogite yields a satisfactory agreement between the model and the observations, the imperfect fit of the kyanite-eclogite (in particular between the calculated and measured grossular content in garnet) calls for exploring this aspect. Figure 17a is a T - $X(\text{H}_2\text{O})$ diagram at 14.5 kbar, corresponding to the pressure inferred in this sample for the growth of the garnet core, for the bulk composition used in calculating Fig. 12. The horizontal axis involves variation of the H_2O content from zero at $X = 0$ to a value sufficient to saturate the assemblages at $X = 1$. When H_2O undersaturation is reached, at $X(\text{H}_2\text{O}) \sim 0.85$, both kyanite and diopside become rapidly stable over the entire temperature interval explored. At lower H_2O contents, first epidote, then quartz disappear from the stable assemblages at $X(\text{H}_2\text{O}) \sim 0.45$ and 0.25, respectively. Consequently, such conditions ($X(\text{H}_2\text{O}) < 0.45$) appear inappropriate to account for the crystallization of the garnet core, which contains quartz and epidote as inclusions. On the other hand, the calculated grossular isopleths become strongly H_2O -sensitive beyond the epidote-out line, decrease to a minimum of about 16 at $X(\text{H}_2\text{O}) \sim 0.15$, and encompass values analysed in the garnet core ($\text{Grs} \sim 21$). In order to explore these divergent signals, a P - T pseudosection has been calculated at $X(\text{H}_2\text{O}) = 0.3$ (Fig. 17b). Nevertheless, epidote is not stable in the entire P - T range explored (650-850 °C, 10-18 kbar). The grossular isopleths (Fig. 17b) fit the values observed in the garnet core, but fail to account for the zoning pattern observed (increase-decrease – see above). Consequently, despite the shortcomings, the H_2O -saturated pseudosection yields the best match between the model and observations for the prograde part of the P - T path of the kyanite-eclogite. Finally, H_2O -saturation is also compatible with the large size of the minerals forming the peak assemblage (garnet, clinopyroxene, amphibole, kyanite) that suggests fast diffusion and hence the presence of a free fluid during the prograde evolution of the rock.

The coarse-grained corundum conundrum

In most kyanite-bearing eclogite in the study area, clusters of acicular corundum grains were produced together with sapphirine and plagioclase in symplectites replacing kyanite (Fig 8b; see also Möller, 1999). Rarely in the field, corundum is

also found as coarser (up to 1 mm) pinkish-violet (Cr-bearing) crystals. They occur as inclusions in 2-4 cm kyanite grains and are thus an earlier generation than the acicular corundum intergrown with plagioclase. Blocky 0.3 mm large corundum crystals, found together with rutile and spinel in one micro-domain of the kyanite-eclogite sample 8023F, are likely of that early generation. At the same time, however, quartz is found locally in the matrix and can form large grains up to 1 mm, although generally confined in clinopyroxene and never in contact with sapphirine or symplectitic corundum. Kyanite, clinopyroxene and quartz are inferred to crystallize in equilibrium on the prograde P - T path (see above). Consequently, corundum could be considered as part of the peak mineral assemblage. Co-stability of quartz, corundum and kyanite would imply unrealistic very high temperatures that are at variance with the other petrological evidence of the rock. Corundum is absent from the calculated pseudosections, even when the bulk Al content is artificially increased. Aluminium is, however, a reputedly slowly diffusing element (e.g. Sautter *et al.*, 1988; McFarlane *et al.*, 2003) and can have very small equilibration volumes. Consequently, we consider that the local presence of coarse-grained corundum, although remaining enigmatic, does not affect the petrological interpretations presented above. It could be caused by (1) minor amounts of Cr and Fe that would stabilize a primary (prograde) corundum, or (2) a local excess of Al in the vicinity of kyanite that would lead to formation of primary corundum.

Tectonic implications

The eclogite-bearing nappe represents a part of the Baltica continental crust that experienced westward tectonic burial to eclogite-facies conditions, beneath the Idefjorden Terrane, followed by eastward, foreland-directed, tectonic exhumation (Möller *et al.*, 2015). In the following section, we discuss the implications of the documented P - T path and the tectonic setting of the Sveconorwegian eclogites.

The first part of the P - T path, retrieved from the core of zoned garnet in the Fe-Ti-rich eclogite, shows a prograde metamorphic evolution from ~ 670 °C / 7 kbar to 720 °C / 8.5 kbar, at typical Barrovian-type conditions. Bent to sigmoidal inclusion trails, from the inner core of the Fe-Ti eclogite garnet, record syntectonic garnet growth during this stage. This was followed by burial to eclogite-facies depths at high temperature, reaching 860-900 °C at 16.5-18 kbar, significantly higher than previous minimum estimations (~ 700 °C / 15 kbar, Möller, 1999) and tightest constrained for the kyanite-eclogite sample. Figure 18 illustrates that the peak pressure conditions were slightly hotter than a “typical” stable continental geotherm, and were reached along a steep prograde path (high dP/dT , ~ 5 °C/km). The steep prograde path is a possible evidence that burial to eclogite facies conditions was a rapid process, so to prevent progressive thermal equilibration.

Subsequent near-isothermal decompression to granulite-facies conditions (810-870 °C, 8-11 kbar) is in accordance with the regional occurrence of high-temperature parageneses, including opx-bearing leucosome in garnet amphibolite, in western parts of the Eastern Segment (e.g. Hansen *et al.*, 2015; Möller *et al.*, 2015; Piñán-Llamas *et al.*, 2015). Granulite- and upper amphibolite-facies tectonites, including sapphirine-bearing mylonites, demonstrate that the decompression was locally coeval with deformation (Möller, 1999; Möller *et al.*, 2015; Tual *et al.*, 2015).

U-Pb zircon ages of prograde eclogitization and partial melt crystallization in orthogneiss place broad age brackets on the decompression at 988 ± 6 Ma and 976 ± 6 Ma, respectively (Möller *et al.*, 2015). However, the preservation of growth zoning in garnet, the near-isothermal decompression path, and the formation of symplectite

suggest rapid exhumation and short residence at high temperatures (cf. Möller, 1998, 1999).

To summarize, the steepness of the P - T path and the peak conditions of up to 900 °C / 18 kbar of the eclogites in the Eastern Segment suggest a rapid burial to ~65 km and a rapid tectonic uplift (Fig. 17). From a tectonic point of view, this firstly requires a scenario with doubled crustal thickness at *c.* 1 Ga (Möller *et al.*, 2015). Secondly, given the geological setting in a migmatized nappe and the high temperatures at peak-pressure conditions and during decompression, it is likely that the exhumation was aided by the presence of partial melt (Möller *et al.*, 2015; Tual *et al.*, 2015).

The clockwise P - T path of the eclogites, associated with near isothermal decompression through granulite-facies conditions is typical of crustal overthickening and continental collision (e.g. Harley, 1989). This scenario is compatible with the setting of the eclogite-bearing nappe and enclosing rocks in the Eastern Segment, where HP-HT conditions, ductile deformation and foreland-vergent flow were widespread (Johansson *et al.*, 1991; Johansson & Kullerud 1993; Wang & Lindh, 1996; Möller *et al.*, 1997, 2007, 2015; Möller, 1998, 1999; Andersson *et al.*, 1999, 2002; Söderlund *et al.*, 2002; Bingen *et al.*, 2008b; Hansen *et al.*, 2015; Piñán-Lamas *et al.*, 2015; Tual *et al.*, 2015).

High-grade eclogite-facies terranes, petrologically almost identical to those in the Sveconorwegian orogen (carrying sapphirine-symplectitic high-temperature overprinted kyanite eclogite), are common in continental collision zones. Examples are found in the Trans-Hudson orogen (Baldwin *et al.*, 2007, 2015), the Grenville orogen (Grant, 1989; Davidson, 1990), the Variscan orogen (O'Brien, 1997; Godard & Mabit, 1998), the Caledonides (Johansson & Möller, 1986; Möller, 1988; Elvevold & Gilotti, 2000; Janák *et al.*, 2013), and the Alps (Liati & Siedel, 1994, 1996; Moulas *et al.*, 2013). The geodynamic setting varies from UHP metamorphism by continental subduction (e.g. Liou *et al.*, 2004 and references therein) to HP metamorphism by crustal thickening (e.g. Grujic *et al.*, 2011).

The classic markers of subduction of the continental crust into the mantle (Mg-Cr-rich mantle peridotite and UHP indicators), present e.g. in the Western Gneiss Region of Norway (Cuthbert *et al.*, 2000), are absent from the eclogite-bearing terrane in the Eastern Segment of the Sveconorwegian orogen. This and the fact that the peak-pressure estimate is only slightly hotter than a stable continental thermal gradient (Fig. 17), argues against subduction into the mantle and instead for a setting where the eclogite-facies metamorphism was caused by thickening of the continental crust.

Among numerous specific models for the formation and exhumation of eclogites, one recently brought forward for the eastern Himalayan eclogites (Grujic *et al.*, 2011; Warren *et al.*, 2011) accounts for some tectonic and metamorphic features that are similar to the eclogites of the Eastern Segment. These similarities include (1) the metamorphic P - T path, with high temperatures (reaching ~850 °C) during eclogite-facies metamorphism (cf. also Kohn, 2014 and references therein); (2) similar compositions of the eclogite-bearing host gneisses and their surroundings (e.g. Hodges, 2000), i.e. crustal affinity and lack of density contrast that could have promoted buoyancy-driven exhumation (Grujic *et al.*, 2011); (3) a ductile thrust at the base of the eclogite-bearing unit that has placed HP rocks on top of lower- P ones (Kelett *et al.*, 2010; Grujic *et al.*, 2011; Warren *et al.*, 2011). Eclogites in eastern Himalaya represent fragments of the lower overthickened crust and have been interpreted as exhumed over a crustal scale ramp within a weak lower crust (Grujic *et*

al., 2011; Warren *et al.*, 2011). This syn-convergence exhumation model involves tectonic extrusion (thrust below coupled with extension zone above) and does not require major extension or buoyancy forces (Grujic *et al.*, 2011). This model constitutes an appealing mechanism for the formation and exhumation of the eclogites in the Eastern Segment (cf. Möller *et al.*, 2015). The similarities between Sveconorwegian and Himalayan eclogite occurrences emphasize the modern style of Grenvillian-aged tectonics.

ACKNOWLEDGEMENTS

L. Tual thanks Matthijs Smit for great assistance and fruitful discussions during EMPA analysis at Copenhagen University, DK. Discussions during an Erasmus teaching mobility of L. Tual at Rennes 1 University were appreciated. Jenny Andersson is thanked for numerous discussions and for the template of Figure 1. Iwona Klonowska and an anonymous reviewer are thanked for constructive reviews and Doug Robinson for careful editorial handling. Research was funded by grants from the Geological Survey of Sweden (60-1655/2009, 61-1420/2010) and the Crafoord Foundation (20110817) to C. Möller.

REFERENCES

- Andersson, J., Söderlund, U., Cornell, D., Johansson, L. & Möller, C., 1999. Sveconorwegian (-Grenvillian) deformation, metamorphism and leucosome formation in SW Sweden, SW Baltic Shield: constraints from a Mesoproterozoic granite intrusion. *Precambrian Research*, **98**, 151-171.
- Andersson, J., Möller, C. & Johansson, L., 2002. Zircon geochronology of migmatite gneisses along the Mylonite Zone (S Sweden): a major Sveconorwegian terrane boundary in the Baltic Shield. *Precambrian Research*, **114**, 121-147.
- Austin Hegardt, E., Cornell, D.H., Claesson, L., Simakov, S., Stein, H.J. & Hannah, J.L., 2005. Eclogites in the central part of the Sveconorwegian, Eastern Segment of the Baltic Shield: support for an extensive eclogite terrane. *Geologiska Föreningens i Stockholm Förhandlingar*, GFF, **127**, 221-232.
- Baldwin, J. A., Powell, R., Williams, M. L. & Goncalves, P., 2007. Formation of eclogite, and reaction during exhumation to mid-crustal levels, Snowbird tectonic zone, western Canadian Shield. *Journal of Metamorphic Geology*, **25**, 953-974.
- Baldwin, J. A., Powell, R., White, R. W. & Štípská, P., 2015. Using calculated chemical potential relationships to account for replacement of kyanite by symplectite in high pressure granulites. *Journal of Metamorphic Geology*, **33**, 311-330.
- Ballèvre, M., Pitra, P. & Bohn, M., 2003. Lawsonite growth in the epidote blueschists from the Ile de Groix (Armorican Massif, France): a potential geobarometer. *Journal of metamorphic Geology*, **21**, 723-735.
- Bingen, B., 1989. Geochemistry of Sveconorwegian augen gneisses from SW Norway at the amphibolite-granulite facies transition. *Norsk geologisk tidsskrift*, **69**, 177-189.
- Bingen, B. & van Breemen, O., 1998. U-Pb monazite ages in amphibolite-to granulite-facies orthogneiss reflect hydrous mineral breakdown reactions: Sveconorwegian Province of SW Norway. *Contributions to Mineralogy and Petrology*, **132**, 336-353.
- Bingen, B., Skår, Ø., Marker, M., Sigmond, E. M., Nordgulen, Ø., Ragnhildstveit, J., Mansfeld, J., Tucker, R. D. & Liégeois, J. P., 2005. Timing of continental building

- in the Sveconorwegian orogen, SW Scandinavia. *Norwegian Journal of Geology*, **85**, 87-116.
- Bingen, B. & Solli, A., 2009. Geochronology of magmatism in the Caledonian and Sveconorwegian belts of Baltica: synopsis for detrital zircon provenance studies. *Norwegian Journal of Geology*, **89**.
- Bingen, B., Nordgulen, Ø. & Viola, G., 2008a. A four-phase model for the Sveconorwegian orogeny, SW Scandinavia. *Norwegian Journal of Geology* **88**, 43–72.
- Bingen, B., Andersson, J., Soderlund, U. & Moller, C., 2008b. The Mesoproterozoic in the Nordic countries. *Episodes*, **31**, 29-34.
- Brown, M., 2014. The contribution of metamorphic petrology to understanding lithosphere evolution and geodynamics. *Geoscience Frontiers*, **5**, 553-569.
- Brown, G. C. & Mussett, A. E., 1993. The continental crust. In: *The Inaccessible Earth*. Springer Netherlands, 186-212
- Carson, C. J., Powell, R. & Clarke, G. L., 1999. Calculated mineral equilibria for eclogites in CaO-Na₂O-FeO-MgO-Al₂O₃-SiO₂-H₂O: application to the Pouébo Terrane, Pam Peninsula, New Caledonia. *Journal of Metamorphic Geology*, **17**, 9-24.
- Coggon, R. & Holland, T.J.B., 2002. Mixing properties of phengitic micas and revised garnet-phengite thermobarometers. *Journal of Metamorphic Geology*, **20**, 683-696.
- Cuthbert, S.J., Carswell, D.A., Krogh-Ravna, E.J. & Wain, A., 2000. Eclogites and eclogites in the Western Gneiss Region, Norwegian Caledonides. *Lithos*, **52**, 165-195.
- Dale, J., Powell, R., White, R. W., Elmer, F. L. & Holland, T. J. B., 2005. A thermodynamic model for Ca-Na clin amphiboles in Na₂O-CaO-FeO-MgO-Al₂O₃-SiO₂-H₂O-O for petrological calculations. *Journal of Metamorphic Geology*, **23**, 771-791.
- Davidson, A., 1990. Evidence for eclogite metamorphism in the southwestern Grenville Province. *Geological Survey of Canada, Paper*, **90-1C**, 113–118.
- Diener, J. F. A., Powell, R., White, R. W. & Holland, T. J. B., 2007. A new thermodynamic model for clino- and orthoamphiboles in Na₂O-CaO-FeO-MgO-Al₂O₃-SiO₂-H₂O-O. *Journal of Metamorphic Geology*, **25**, 631-656.
- Elvevold, S. & Gilotti, J. A., 2000. Pressure–temperature evolution of retrogressed kyanite eclogites, Weinschenk Island, north–east Greenland Caledonides. *Lithos*, **53**, 127-147.
- Engvik, A. K., Bingen, B. & Solli, A., 2016. Localized occurrences of granulite: *P–T* modeling, U–Pb geochronology and distribution of early-Sveconorwegian high-grade metamorphism in Bamble, South Norway. *Lithos*, **240**, 84-103.
- Godard, G. & Mabit, J. L., 1998. Peraluminous sapphirine formed during retrogression of a kyanite-bearing eclogite from Pays de Léon, Armorican Massif, France. *Lithos*, **43**, 15-29.
- Grant, S. M., 1989. Tectonic implications from sapphirine-bearing lithologies, southwest Grenville Province, Canada. *Journal of Metamorphic Geology*, **7**, 583-598.
- Green, E. C. R., White, R. W., Diener, J. F. A., Powell, R., Holland, T. J. B. & Palin, R. M., 2016. Activity–composition relations for the calculation of partial melting equilibria in metabasic rocks. *Journal of Metamorphic Geology*, **34**, 845-869.
- Grujic, D., Warren, C. J. & Wooden, J. L., 2011. Rapid synconvergent exhumation of Miocene-aged lower orogenic crust in the eastern Himalaya. *Lithosphere*, **3**, 346-366.

- Guiraud, M., Powell, R. & Cottin, J. Y., 1996. Hydration of orthopyroxene—cordierite-bearing assemblages at Laouni, Central Hoggar, Algeria. *Journal of Metamorphic Geology*, **14**, 467-476.
- Guiraud, M., Powell, R. & Rebay, G., 2001. H₂O in metamorphism and unexpected behaviour in the preservation of metamorphic mineral assemblages. *Journal of Metamorphic Geology*, **19**, 445-454.
- Hansen, E., Johansson, L., Andersson, J., LaBarge, L., Harlov, D., Möller, C. & Vincent, S., 2015. Partial melting in amphibolites in a deep section of the Sveconorwegian Orogen, SW Sweden. *Lithos*, **236**, 27-45.
- Harley, S. L., 1989. The origins of granulites: a metamorphic perspective. *Geological Magazine*, **126**, 215-247.
- Hodges, K. V., 2000. Tectonics of the Himalaya and southern Tibet from two perspectives. *Geological Society of America Bulletin*, **112**, 324-350.
- Holland, T. J. B. & Powell, R., 1998. An internally consistent thermodynamic dataset for phases of petrological interest. *Journal of Metamorphic Geology*, **16**, 309-343.
- Holland, T. J. B. & Powell, R., 2003. Activity-composition relations for phases in petrological calculations: an asymmetric multicomponent formulation. *Contributions to Mineralogy and Petrology*, **145**, 492-501.
- Holland, T. J. B. & Powell, R., 2011. An improved and extended internally consistent thermodynamic dataset for phases of petrological interest, involving a new equation of state for solids. *Journal of Metamorphic Geology*, **29**, 333-383.
- Holland, T. J. B., Baker, J. M. & Powell, R., 1998. Mixing properties and activity-composition relationships of chlorites in the system MgO-FeO-Al₂O₃-SiO₂-H₂O. *European Journal of Mineralogy*, **10**, 395-406.
- Janák, M., Krogh Ravn, E. J., Kullerud, K., Yoshida, K., Milovský, R. & Hirajima, T., 2013. Discovery of diamond in the Tromsø Nappe, Scandinavian Caledonides (N. Norway). *Journal of Metamorphic Geology*, **31**, 691-703.
- Johansson, L. & Möller, C., 1986. Formation of sapphirine during retrogression of a basic high-pressure granulite, Roan, Western Gneiss Region, Norway. *Contributions to Mineralogy and Petrology*, **94**, 29-41.
- Johansson, L. & Kullerud, L., 1993. Late Sveconorwegian metamorphism and deformation in southwestern Sweden. *Precambrian Research*, **64**, 347-360.
- Johansson, L., Lindh, A. & Möller, C., 1991. Late Sveconorwegian (Grenville) high-pressure granulite facies metamorphism in southwest Sweden. *Journal of Metamorphic Geology*, **9**, 283-292.
- Johansson, L., Möller, C. & Söderlund, U., 2001. Geochronology of eclogite facies metamorphism in the Sveconorwegian Province of SW Sweden. *Precambrian Research*, **106**, 261-275.
- Kellett, D. A., Grujic, D., Warren, C., Cottle, J., Jamieson, R. & Tenzin, T., 2010. Metamorphic history of a syn-convergent orogen-parallel detachment: The South Tibetan detachment system, Bhutan Himalaya. *Journal of Metamorphic Geology*, **28**, 785-808.
- Kohn, M. J., 2014. Himalayan metamorphism and its tectonic implications. *Annual Review of Earth and Planetary Sciences*, **42**, 381-419.
- Leake, B. E., Woolley, A. R., Arps, C. E. S., *et al.*, 1997. Nomenclature of amphiboles: Report of the Subcommittee on Amphiboles of the International Mineralogical Association, Commission on New Minerals and Mineral Names. *American Mineralogist*, **82**, 1019-1037.
- Leake, B. E., Woolley, A. R., Birch, W. D., Burke, E. A., Ferraris, G., Grice, J. D., Hawthorne, F. C. Kisch, H. J., Krivovichev, V. G., Schumacher, J. C.,

- Stephenson, N. C. N. & Whittaker, E. J., 2004. Nomenclature of amphiboles: additions and revisions to the International Mineralogical Association's amphibole nomenclature. *Mineralogical Magazine*, **68**, 209-215.
- Liati, A. & Seidel, E., 1994. Sapphirine and högbomite in overprinted kyanite-eclogites of central Rhodope, N. Greece: first evidence of granulite-facies metamorphism. *European Journal of Mineralogy*, **6**, 733-737.
- Liati, A. & Seidel, E., 1996. Metamorphic evolution and geochemistry of kyanite eclogites in central Rhodope, northern Greece. *Contributions to Mineralogy and Petrology*, **123**, 293-307.
- Liou, J. G., Tsujimori, T., Zhang, R. Y., Katayama, I. & Maruyama, S., 2004. Global UHP metamorphism and continental subduction/collision: the Himalayan model. *International Geology Review*, **46**, 1-27.
- López-Carmona, A., Pitra, P. & Abati, J., 2013. Blueschist-facies metapelites from the Malpica-Tui Unit (NW Iberian Massif): phase equilibria modelling and H₂O and Fe₂O₃ influence in high-pressure assemblages. *Journal of Metamorphic Geology*, **31**, 263-280.
- McFarlane, C. R. M., Carlson, W. D. & Connelly, J. N., 2003. Prograde, peak, and retrograde P–T paths from aluminium in orthopyroxene: High-temperature contact metamorphism in the aureole of the Makhavinekh Lake Pluton, Nain Plutonic Suite, Labrador. *Journal of Metamorphic Geology*, **21**, 405-423.
- Moulas, E., Kostopoulos, D., Connolly, J. A. & Burg, J. P., 2013. P–T estimates and timing of the sapphirine-bearing metamorphic overprint in kyanite eclogites from Central Rhodope, northern Greece. *Petrology*, **21**, 507-521.
- Möller, C., 1988. Geology and metamorphic evolution of the Roan area, Vestranden, Western Gneiss region, central Norwegian Caledonides. *Norges Geologiske Undersøkelse*.
- Möller, C., 1998. Decompressed eclogites in the Sveconorwegian (–Grenvillian) orogen of SW Sweden: petrology and tectonic implications. *Journal of Metamorphic Geology*, **16**, 641-656.
- Möller, C., 1999. Sapphirine in SW Sweden: a record of Sveconorwegian (–Grenvillian) late-orogenic tectonic exhumation. *Journal of Metamorphic Geology*, **17**, 127–141.
- Möller, C., Andersson, J., Lundqvist, I. & Hellström, F.A., 2007. Linking deformation, migmatite formation and zircon U–Pb geochronology in poly-metamorphic orthogneisses, Sveconorwegian Province, Sweden. *Journal of Metamorphic Geology*, **25**, 727–775.
- Möller, C., Andersson, J., Dyck, B. & Antal Lundin, I., 2015. Exhumation of an eclogite terrane as a hot migmatitic fold nappe, Sveconorwegian orogen. Hirajama, T., Medaris, G. (Eds.), High- and ultrahigh-pressure metamorphism, from microscopic to orogenic scale. Lithos (Special Issue). *Lithos*, **226**, 147–168.
- O'Brien, P. J., 1997. Garnet zoning and reaction textures in overprinted eclogites, Bohemian Massif, European Variscides: a record of their thermal history during exhumation. *Lithos*, **41**, 119-133.
- Pattison, D. R. M., 2003. Petrogenetic significance of orthopyroxene-free garnet + clinopyroxene + plagioclase ± quartz-bearing metabasites with respect to the amphibolite and granulite facies. *Journal of Metamorphic Geology*, **21**, 21-34.
- Peterson, A., Scherstén, A., Bingen, B., Gerdes, A. & Whitehouse, M. J., 2015. Mesoproterozoic continental growth: U–Pb–Hf–O zircon record in the Idefjorden Terrane, Sveconorwegian Orogen. *Precambrian Research*, **261**, 75-95.

- Piñán-Llamas, A., Andersson, J. & Möller, C., 2015. Polyphasal foreland-vergent deformation in a deep parautochthonous section of the 1 Ga Sveconorwegian orogen, in: Roberts, N., Viola, G., Slagstad, T. (Eds.), The structural, metamorphic and magmatic evolution of Mesoproterozoic orogens. *Precambrian Research*, **265**, 121-149.
- Pitra, P., Kouamelan, A. N., Ballèvre, M. & Peucat, J.-J., 2010. Palaeoproterozoic high-pressure granulite overprint of the Archean continental crust: evidence for homogeneous crustal thickening (Man Rise, Ivory Coast). *Journal of Metamorphic Geology*, **28**, 41-58.
- Powell, R. (1983). Processes in granulite-facies metamorphism. *Migmatites, melting and metamorphism*, 127-139.
- Powell, R. & Holland, T., 1990. Calculated mineral equilibria in the pelite system, KFMASH. *American Mineralogist*, **75**, 367-380.
- Powell, R., Holland, T. J. B. H. & Worley, B., 1998. Calculating phase diagrams involving solid solutions via non-linear equations, with examples using THERMOCALC. *Journal of metamorphic Geology*, **16**, 577-588.
- Sautter, V., Jaoul, O. & Abel, F., 1988. Aluminum diffusion in diopside using the $^{27}\text{Al}(p,\gamma)^{28}\text{Si}$ nuclear reaction: preliminary results. *Earth and Planetary Science Letters*, **89**, 109-114.
- Slagstad, T., Roberts, N. M., Marker, M., Røhr, T. S. & Schiellerup, H., 2012. A non-collisional, accretionary Sveconorwegian orogen. *Terra Nova*, **25**, 30-37.
- Spear, F. S., 1993 Metamorphic phase equilibria and pressure-temperature-time paths. Mineralogical Society of America, Washington, 799 pp.
- Stephens, M. B., 2009. Synthesis of the bedrock geology in the Bergslagen region, Fennoscandian Shield, south-central Sweden. *Sveriges geologiska undersökning (SGU)*.
- Stephens, M. B. & Andersson, J., 2015. Migmatization related to mafic underplating and intra-or back-arc spreading above a subduction boundary in a 2.0–1.8 Ga accretionary orogen, Sweden. *Precambrian Research*, **264**, 235-257.
- Söderlund, U., Jarl, L.G., Persson, P.O., Stephens, M.B. & Wahlgren, C.A.-H., 1999. Protolith ages and timing of deformation in the eastern, marginal part of the Sveconorwegian orogen, southwestern Sweden. *Precambrian Research*, **94**, 29–48.
- Söderlund, U., Möller, C., Andersson, J., Johansson, L. & Whitehouse, M.J., 2002. Zircon geochronology in polymetamorphic gneisses in the Sveconorwegian orogen, SW Sweden: ion microprobe evidence for 1.46-1.42 Ga and 0.98-0.96 Ga reworking. *Precambrian Research*, **113**, 193-225.
- Söderlund, U., Hellström, F. A. & Kamo, S. L., 2008. Geochronology of high-pressure mafic granulite dykes in SW Sweden: tracking the P – T – t path of metamorphism using Hf isotopes in zircon and baddeleyite. *Journal of Metamorphic Geology*, **26**, 539-560.
- Tual, L., Pinan-Llamas, A. & Möller, C., 2015. High-Temperature Deformation in the Basal Shear Zone of an Eclogite-Bearing Fold Nappe, Sveconorwegian Orogen, Sweden, in: Roberts, N., Viola, G., Slagstad, T. (Eds.), The structural, metamorphic and magmatic evolution of Mesoproterozoic orogens. *Precambrian Research*, **265**, 104-120.
- Vander Auwera, J., Bolle, O., Bingen, B., Liégeois, J. P., Bogaerts, M., Duchesne, J. C. & Longhi, J., 2011. Sveconorwegian massif-type anorthosites and related granitoids result from post-collisional melting of a continental arc root. *Earth-Science Reviews*, **107**, 375-397.

- Vielzeuf, D. & Schmidt, M. W., 2001. Melting relations in hydrous systems revisited: application to metapelites, metagreywackes and metabasalts. *Contributions to Mineralogy and Petrology*, **141**, 251-267.
- Wahlgren, C. H., Cruden, A. R. & Stephens, M. B., 1994. Kinematics of a major fan-like structure in the eastern part of the Sveconorwegian orogen, Baltic Shield, south-central Sweden. *Precambrian Research*, **70**, 67-91.
- Wang, X.-D. & Lindh, A., 1996. Temperature-pressure investigation of the southern part of the Southwest Swedish Granulite Region. *European Journal Mineralogy*, **8**, 51-67
- Warren, C. J., Grujic, D., Kellett, D. A., Cottle, J., Jamieson, R. A. & Ghalley, K. S., 2011. Probing the depths of the India-Asia collision: U-Th-Pb monazite chronology of granulites from NW Bhutan. *Tectonics*, **30**, TC2004.
- White, R. W., Powell, R., Holland, T. J. B. & Worley, B. A., 2000. The effect of TiO₂ and Fe₂O₃ on metapelitic assemblages at greenschist and amphibolite facies conditions: mineral equilibria calculations in the system K₂O-FeO-MgO-Al₂O₃-SiO₂-H₂O-TiO₂-Fe₂O₃. *Journal of Metamorphic Geology*, **18**, 497-511.
- White, R. W., Powell, R. & Holland, T. J. B., 2001. Calculation of partial melting equilibria in the system Na₂O-CaO-K₂O-FeO-MgO-Al₂O₃-SiO₂-H₂O (NCKFMASH). *Journal of Metamorphic Geology*, **19**, 139-153.
- White, R. W., Powell, R. & Clarke, G. L., 2002 The interpretation of reaction textures in Fe-rich metapelitic granulites of the Musgrave Block, central Australia: constraints from mineral equilibria calculations in the system K₂O-FeO-MgO-Al₂O₃-SiO₂-H₂O-TiO₂-Fe₂O₃. *Journal of Metamorphic Geology*, **20**, 41-55.
- White, R. W., Powell, R. & Holland, T. J. B., 2007 Progress relating to calculation of partial melting equilibria for metapelites. *Journal of Metamorphic Geology*, **25**, 511-527.
- Wolf, M. B. & Wyllie, P. J., 1994. Dehydration-melting of amphibolite at 10 kbar: the effects of temperature and time. *Contributions to Mineralogy and Petrology*, **115**, 369-383.

SUPPORTING INFORMATION

Figure S1: Pseudosection calculated for the kyanite eclogite (8023F), ignoring Fe fractionation in sulphide. The rock composition is given as mole-% oxide. Compositional isopleths for garnet and clinopyroxene are shown in red and green, respectively.

Figure S2: T-X(Fe₂O₃) pseudosection showing the effect of Fe₂O₃ (a) on the paragenesis at 14 kbar, between 610 and 830 °C, for the kyanite-eclogite sample 8023F – Fractionation of Fe in sulphide is not considered. The bulk rock compositions in mole-% oxide corresponding to minimum and maximum possible amount of Fe₂O₃ ($X = 0$ and $X = 1$, respectively) are given in the upper right. The pseudosection is calculated in the range of $X = 0$ and $X = 1$. The white line marks the Fe₂O₃ value corresponding to the measured Fe₂O₃. (b) P - T pseudosection showing the effect of increasing Fe₂O₃, using a value corresponding at $X = 0.37$ in (a).

FIGURES CAPTIONS

Figure 1: Sketch map of the Sveconorwegian orogen showing the Eastern Segment (dark grey tones) and western Sveconorwegian terranes (white), separated by ductile

deformation zones (terrane divisions after Bingen *et al.*, 2008a; extent of Sveconorwegian magmatism in Telemarkia after Slagstad *et al.*, 2012). Figure based on 1:5 M Fennoscandian map database and Geological Survey of Sweden 1:1 M Bedrock map database, template provided by J. Andersson. TIB – Transscandinavian Igneous Belt.

Figure 2: Sketch map showing the eclogite-bearing terrane in the Eastern Segment, after Möller *et al.* (2015); parts of this map are based on regular bedrock map data from the Geological Survey of Sweden). Locations of the investigated samples (MU6, 8023F) are indicated.

Figure 3: Photomicrographs of textures in the investigated samples. (a) Fe-Ti-rich eclogite (MU6) with the high-pressure assemblage garnet + quartz + clinopyroxene + rutile. Clinopyroxene (cpx) is partly replaced by amphibole (hb; dark brown-green). Rutile (ru) is partly to completely replaced by ilmenite (ilm) in the matrix. (b) Kyanite eclogite (8023F) with a relict high-pressure assemblage kyanite + garnet + clinopyroxene + pargasitic amphibole (hb). Dark fine-grained domains are symplectite of sapphirine + plagioclase ± corundum. They locally rim relict kyanite and are surrounded by plagioclase.

Figure 4: Texture and chemical composition of garnet in Fe-Ti-rich eclogite sample MU6. (a) Photomicrograph of a garnet crystal with oriented inclusion trails of rutile and quartz in the core (internal foliation S_i) and unoriented inclusions in the rim. Inclusion trails in the core show a slight bend suggesting syntectonic growth of the crystal. The green arrow marks the garnet profile in (b). (b) Profile across garnet in (a) showing chemical zoning in garnet. (c, d, e) X-ray maps of another garnet showing the relative concentration in major elements.

Figure 5: Textures and mineral compositions in Fe-Ti-rich eclogite sample MU6. (a) Back-scattered electron (BSE) image of clinopyroxene with plagioclase and quartz inclusions. Compositions of clinopyroxene (upper right) and plagioclase (left) analyzed at the color-coded dots. (b) Photomicrograph showing replacement of matrix clinopyroxene by amphibole (hb). Rutile, originally hosted in clinopyroxene, is surrounded by ilmenite. (c) BSE image of rutile and amphibole (hb) inclusions in garnet. (d) Amphibole compositions in different textural settings. Classification after Leake *et al.* (1997; 2004). (e) BSE image of quartz and plagioclase inclusion in garnet core. (f) Ternary plot showing the variation of plagioclase composition according to their textural setting. The composition of plagioclase inclusions in garnet cores varies from bytownite to andesine; plagioclase expelled from clinopyroxene varies from labradorite to andesine. (g) Photomicrograph illustrating the increase of rutile grain size from garnet core to rim and matrix. (h) Photomicrograph showing partial replacement of matrix rutile by ilmenite.

Figure 6: Texture and chemical composition of garnet in kyanite eclogite sample 8023F. (a) BSE image of garnet grain with inclusions of kyanite, zoisite (ep), and quartz. Garnet is locally rimmed by an amphibole (hb) + plagioclase corona. (b) Profile across garnet showing chemical zoning. (c, d, e) X-ray maps of garnet showing the relative concentration of major elements. White arrow in (c) marks the profile in (b).

Figure 7: Photomicrograph (PPL) of a clinopyroxene crystal with plagioclase expelled along crystallographic planes (less abundant in the crystal core). Three profiles show the compositional variation across the grain, notably a decrease of jadeite content from core to rim.

Figure 8: Textures in kyanite eclogite sample 8023F. (a) BSE image of typical reaction textures involving replacement of kyanite. A remnant crystal of kyanite is present in the core of a fine-grained symplectite of sapphirine + plagioclase. (b) PPL photomicrograph of symplectitic sapphirine + plagioclase + corundum. Late saussurite appears as faint clouding of plagioclase.

Figure 9: Mineral compositional diagrams of plagioclase, clinopyroxene and amphibole from the kyanite-eclogite sample 8023F. (a) Ternary plots show the variation of plagioclase and clinopyroxene composition in different textural settings. See text for details. (b) Amphibole composition in different textural settings. Classification after Leake *et al.*, (1997; 2004).

Figure 10: Textures in kyanite eclogite 8023F. Photomicrograph (a) and BSE image (b) of typical reaction rim between garnet and clinopyroxene. Symplectite of plagioclase + amphibole surrounds garnet, while plagioclase + orthopyroxene rims clinopyroxene. Clinopyroxene contains expelled plagioclase blebs. A sapphirine + plagioclase symplectite in (a) indicates the former presence of kyanite. The graphs in (b) show the composition of plagioclase (An ; upper left, from garnet rim to clinopyroxene core) and the composition of clinopyroxene (Jd , X_{Fe} ; upper right). (c) BSE image of a rare “secondary inclusion” in garnet showing orthopyroxene + plagioclase + quartz, inferred as a pseudomorph of a clinopyroxene inclusion in garnet.

Figure 11: Pseudosection calculated for the Fe-Ti-rich eclogite (MU6). The rock composition is given as mole % oxide. Arrows indicate the interpreted P - T path, and ellipses represent the following features: (1a) onset of garnet growth and formation of the inclusion-rich garnet core, (1b) onset of growth of the inclusion-free outer core of garnet, (1c) onset of growth of the inclusion-rich inner rim of garnet, (2) equilibrated matrix assemblage and outer rim of garnet; (3) formation of symplectitic reaction rims and associated local reequilibration. (b) Isoleths of grossular (Grs) and X_{Fe} in garnet. (c) Isoleths of X_{Fe} and Jd in clinopyroxene and An in plagioclase.

Figure 12: Pseudosection calculated for the kyanite eclogite (8023F). The rock composition is given as mole-% oxide. Ellipse 1 represents the onset of M1 (prograde growth of garnet cores); the yellow field highlights the assemblage present as inclusions in garnet. Ellipse 2 corresponds to the M2 peak assemblage and composition of garnet (yellow) and clinopyroxene (green). Compositional isopleths of grossular (Grs) and X_{Fe} in garnet are shown in (b) and isopleths X_{Fe} and Jd in clinopyroxene in (c).

Figure 13: Pseudosection calculated for the kyanite eclogite (8023F; same as Figure 12) showing modal proportions of the major minerals in volume % (garnet, clinopyroxene, amphibole, kyanite). The ellipse marks the intersection of mineral volume modes estimated from the thin section.

Figure 14: Effect of Fe^{2+} fractionation due to the presence of sulphides in the kyanite eclogite sample 8023F. (a) Pseudosection calculated with the analyzed whole-rock composition without taking into account the fractionation of Fe^{2+} in sulphides. (b) Pseudosection from (a) as a background image with superposition of kyanite-, garnet- and diopside-in lines for a composition of which Fe^{2+} contained in sulphides was subtracted. The main effect is the shift of kyanite- and diopside-in lines to higher temperature (up to 40 °C) and the garnet-in line to higher pressure (up to 1.5 kbar).

Figure 15: P - $X(\text{Fe}_2\text{O}_3)$ pseudosection showing the effect of varying the proportion of Fe_2O_3 vs. FeO on assemblages at 760 °C, between 8 and 18 kbar, for the Fe-Ti-rich eclogite sample MU6. The bulk rock compositions in mole% oxide corresponding to minimum and maximum possible amounts of Fe_2O_3 ($X = 0$ and 1, respectively) are given in the upper right. The pseudosection is calculated in the range of $X = 0$ and $X = 0.5$. The white line shows the measured Fe_2O_3 value.

Figure 16: P - $X(\text{Fe}_2\text{O}_3)$ pseudosection showing the effect of Fe_2O_3 on the assemblages at 800 °C, between 12 and 14 kbar, for the kyanite-eclogite sample 8023F. The bulk rock compositions in mole % oxide corresponding to minimum and maximum possible amount of Fe_2O_3 ($X = 0$ and 1, respectively) are given in the upper right. The pseudosection is calculated in the range of $X = 0$ and $X = 0.40$. The white line marks the measured Fe_2O_3 value. See text for details.

Figure 17: Effect of H_2O on the pseudosection of the kyanite-eclogite sample 8023F. (a) T - $X(\text{H}_2\text{O})$ pseudosection calculated between 675 and 825 °C at 14.5 kbar. The white line marks the H_2O value chosen to calculate the P - T pseudosection in (b). Grossular isopleths become strongly H_2O -sensitive beyond the epidote-out line and decrease with decreasing H_2O content. (b) P - T pseudosection calculated for an H_2O -undersaturated composition ($X = 0.3$ in (a)). See text for details.

Figure 18: P - T path for Sveconorwegian eclogite, based on the modelling presented in this study. Ages of eclogitization are from Möller *et al.* (2015). Metamorphic facies from Spear (1993), with “typical” stable continental geotherm from Brown & Musset (1993). Z = Zeolite; P-P = Prehnite-pumpellyite; B = Blueschist; GS = Greenschist; E-A = Epidote-amphibolite; E = Eclogite; A = Amphibolite; G = Granulite.

TABLE CAPTIONS

Table 1: Representative mineral analyses from the Fe-Ti eclogite (MU6) and the kyanite eclogite (8023F). inc. = inclusion in; mat. = matrix; out. = outer; coro. = corona; sy. = symplectite; exp. = expelled; c. = close to; reint = reintegrated clinopyroxene (domanial composition of diopside + plagioclase). $X_{Fe} = \text{Fe}^{2+}/(\text{Fe}^{2+}+\text{Mg})$; $X_{Grs} = \text{Ca}/(\text{Ca}+\text{Fe}^{2+}+\text{Mg}+\text{Mn})$; $X_{Prp} = \text{Mg}/(\text{Ca}+\text{Fe}^{2+}+\text{Mg}+\text{Mn})$; $X_{Alm} = \text{Fe}^{2+}/(\text{Ca}+\text{Fe}^{2+}+\text{Mg}+\text{Mn})$; $X_{Sps} = \text{Mn}/(\text{Ca}+\text{Fe}^{2+}+\text{Mg}+\text{Mn})$; $X_{An} = \text{Ca}/(\text{Ca}+\text{Na}+\text{K})$; $X_{Jd} = \text{Na}/(\text{Na}+\text{Ca})$; $X_{CaTs} = \text{Al}^{\text{IV}}-X_{Jd}$; $X_{Or} = \text{K}/(\text{Ca}+\text{Na}+\text{K})$; Fe-Ti eclogite (MU6): (a) garnet and clinopyroxene (b) plagioclase and amphibole. Kyanite eclogite (8023F): (c) garnet and clinopyroxene. (d) orthopyroxene, spinel, sapphirine, plagioclase, epidote and amphibole.

Table 2: Bulk composition of the two studied samples (wt. %). Fe_2O_3^* – total Fe expressed as Fe_2O_3 . FeO – measured by titration

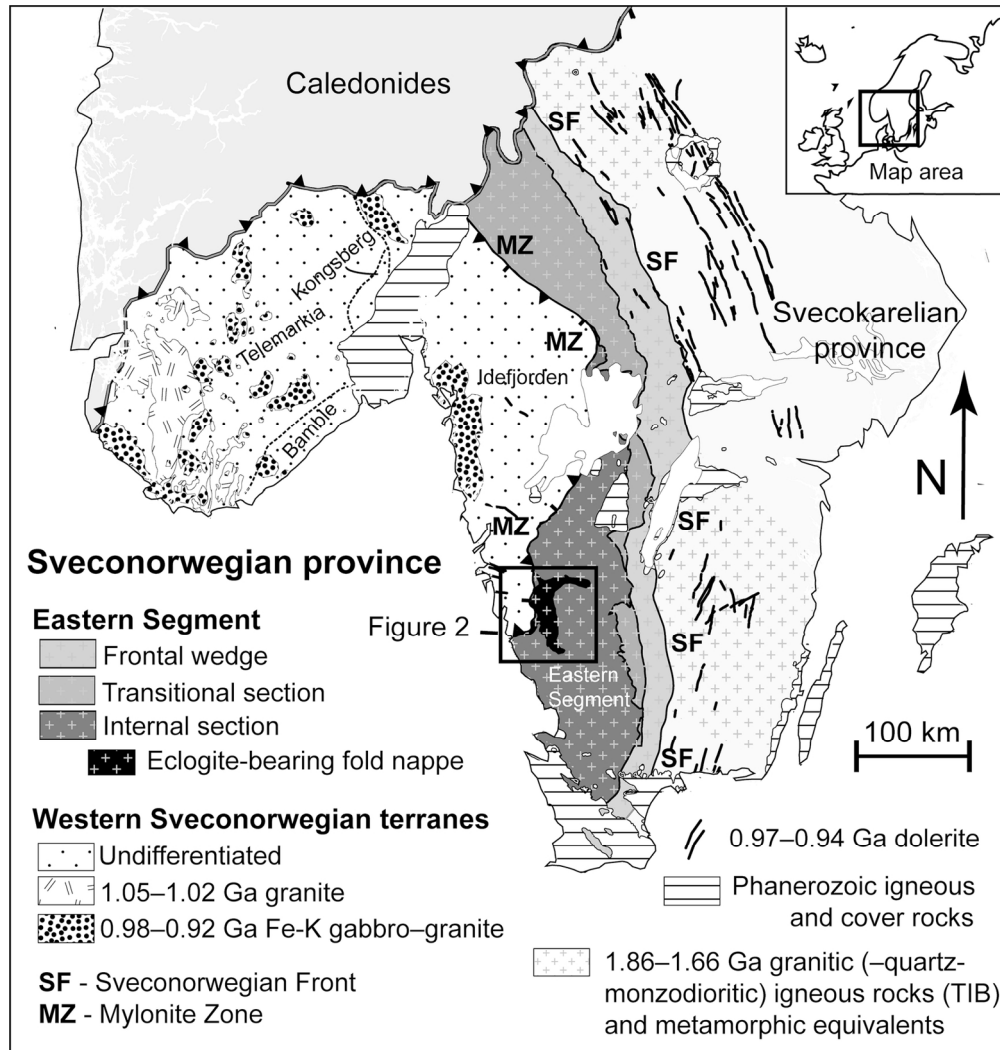


Figure 1: Sketch map of the Sveconorwegian orogen – 80mm

146x153mm (300 x 300 DPI)

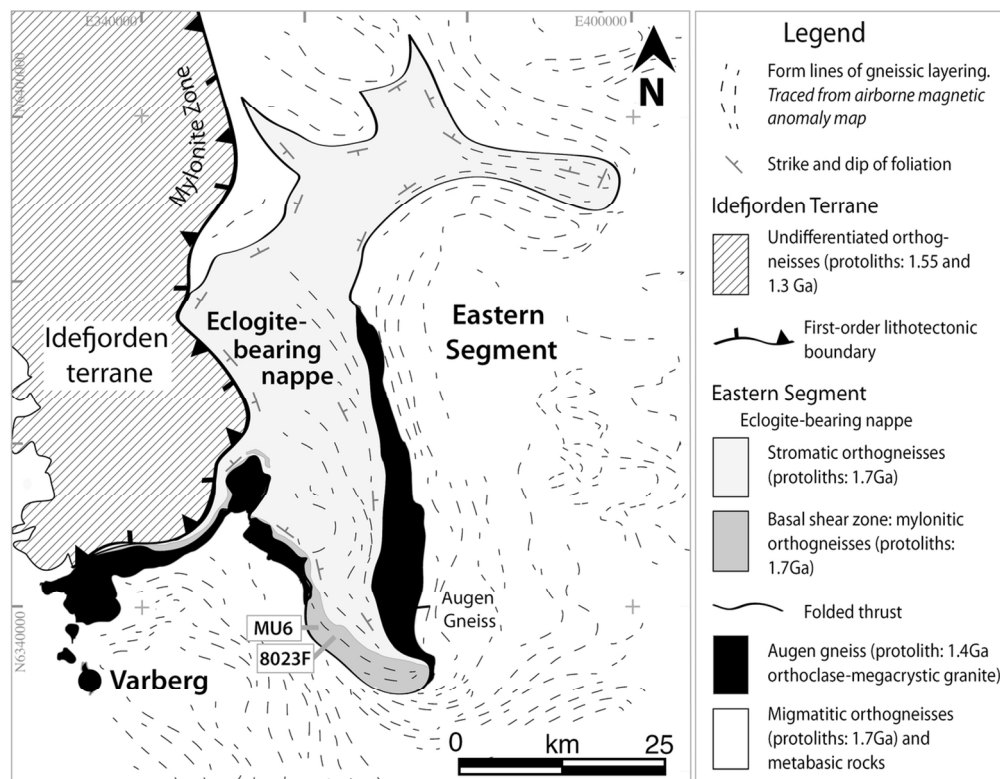


Figure 2: Sketch map showing the eclogite-bearing terrane in the Eastern Segment – 120mm

113x88mm (300 x 300 DPI)

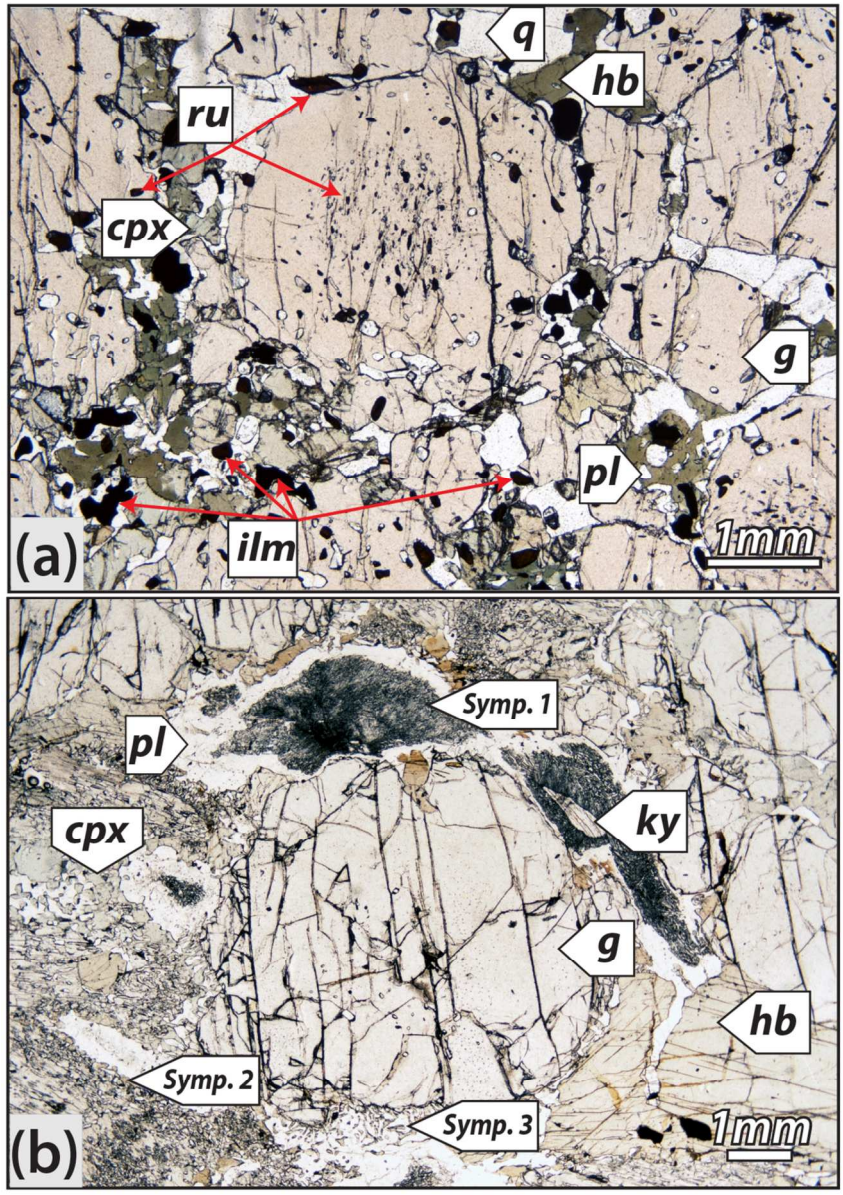


Figure 3: Photomicrographs of textures in the investigated samples - 80mm
111x157mm (300 x 300 DPI)

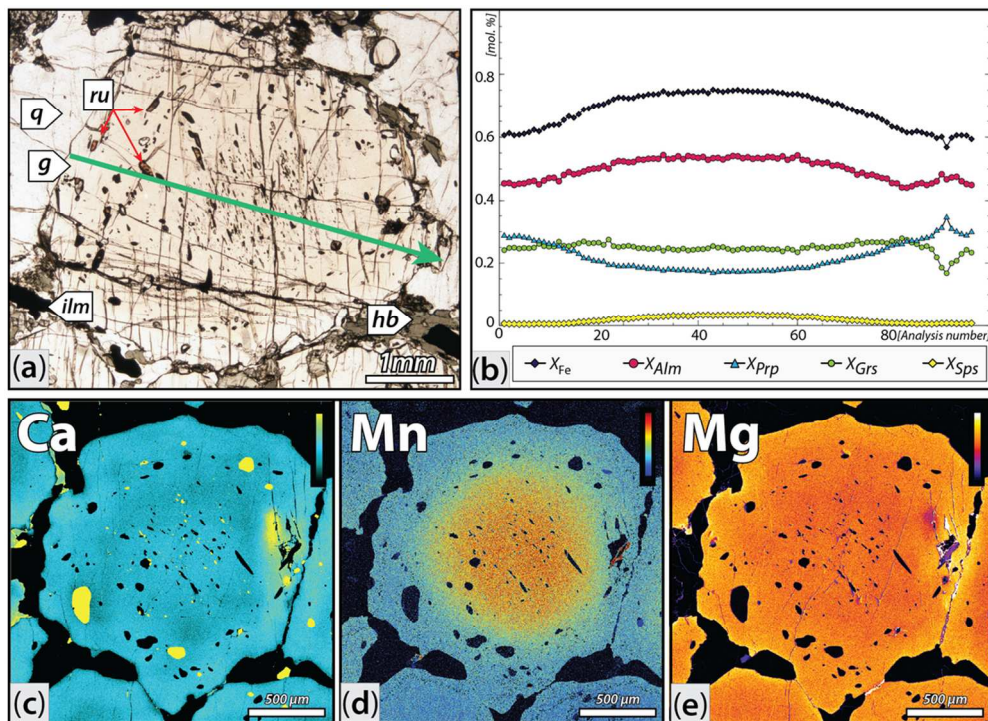


Figure 4: Texture and chemical composition of garnet in Fe-Ti-rich eclogite sample MU6. – 170mm
102x74mm (300 x 300 DPI)

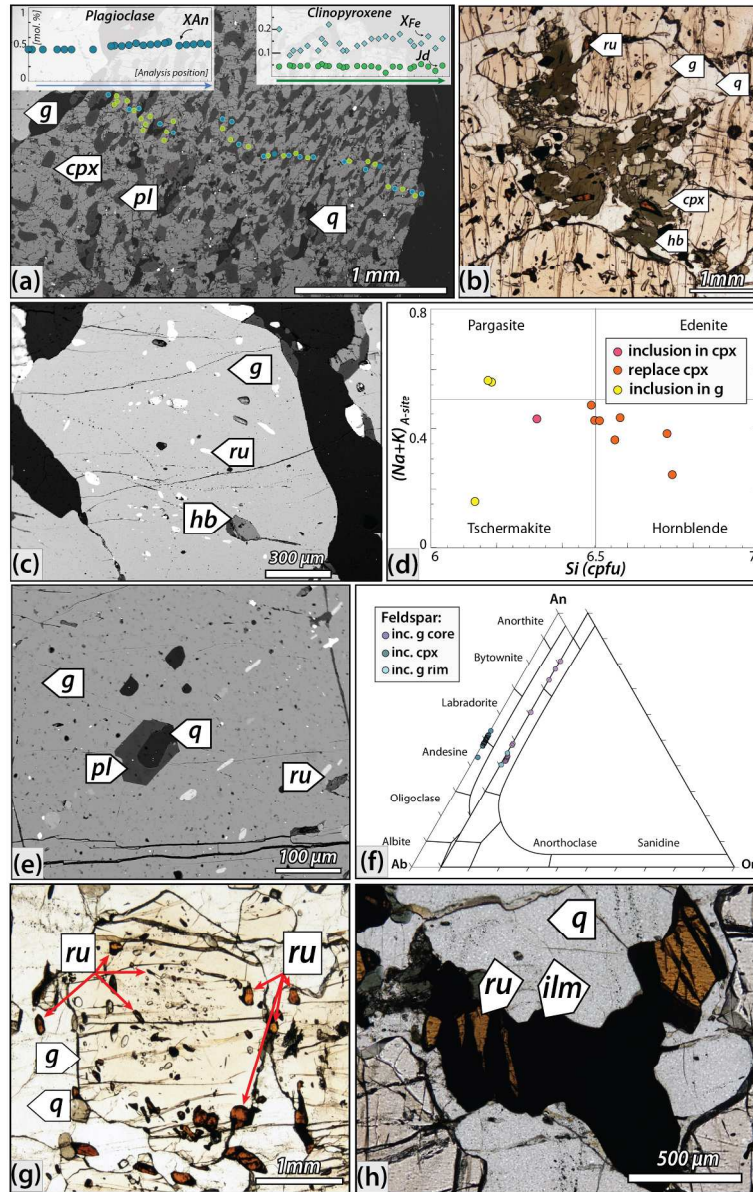


Figure 5: Textures and mineral compositions in Fe-Ti-rich eclogite sample MU6. – 170mm

234x366mm (300 x 300 DPI)

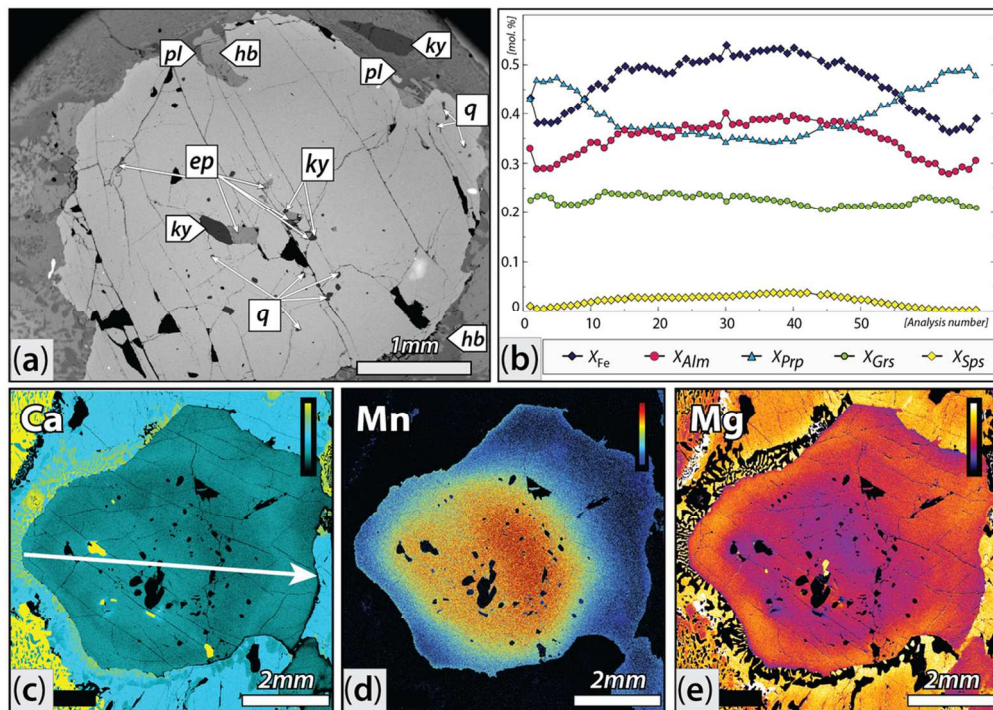


Figure 6: Texture and chemical composition of garnet in kyanite eclogite sample 8023F. – 170mm
101x72mm (300 x 300 DPI)

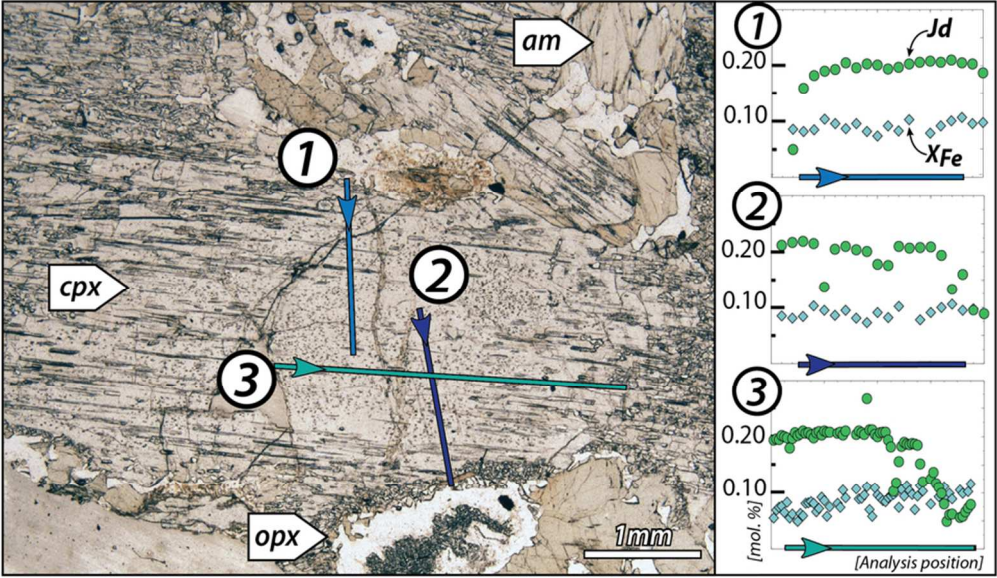


Figure 7: Photomicrograph (PPL) of a clinopyroxene crystal – 140mm

81x47mm (300 x 300 DPI)

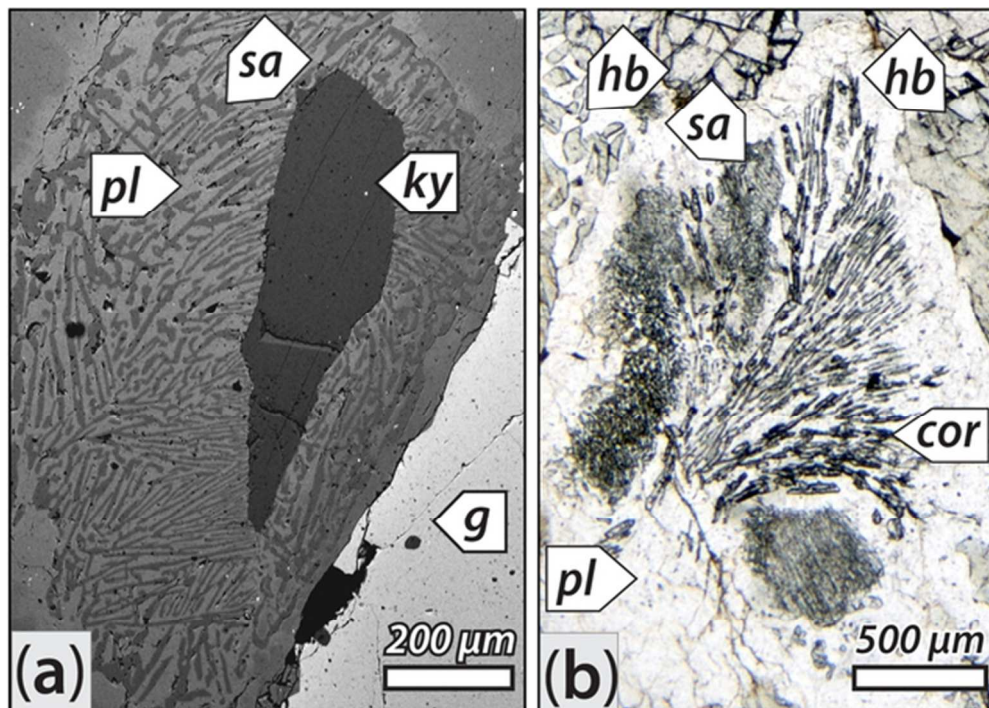


Figure 8: Textures in kyanite eclogite sample 8023F. – 80mm

54x38mm (300 x 300 DPI)

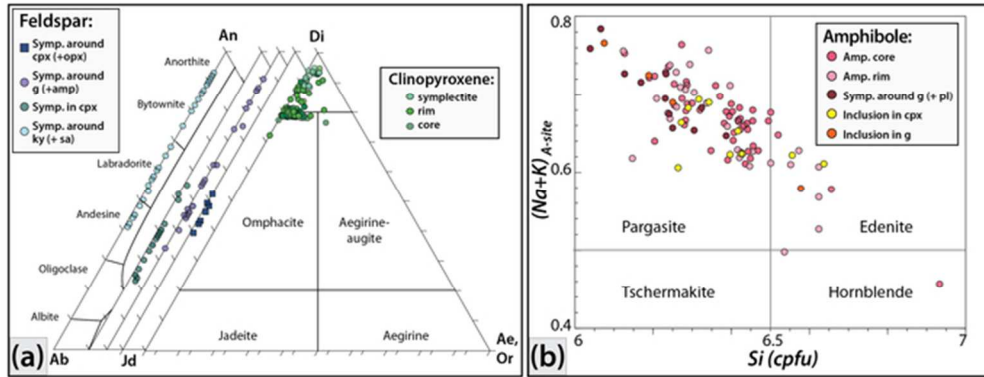


Figure 9: Mineral compositional diagrams of plagioclase, clinopyroxene and amphibole from the kyanite-eclogite sample 8023F. – 170mm

58x22mm (300 x 300 DPI)

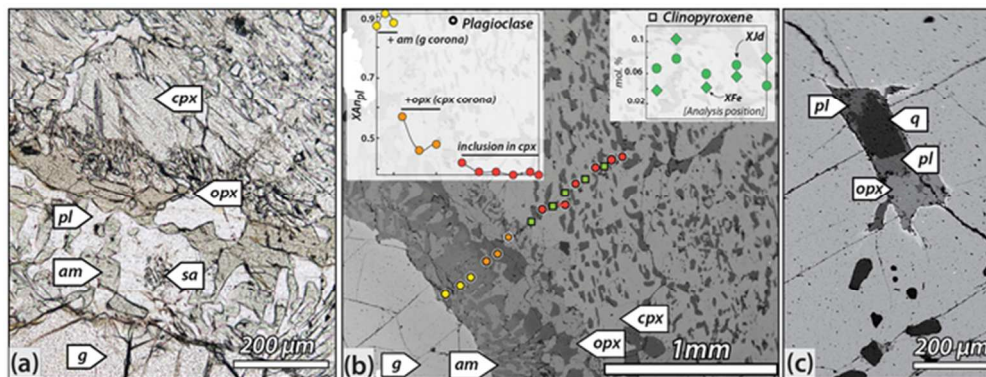


Figure 10: Textures in kyanite eclogite 8023F. – 170mm

58x22mm (300 x 300 DPI)

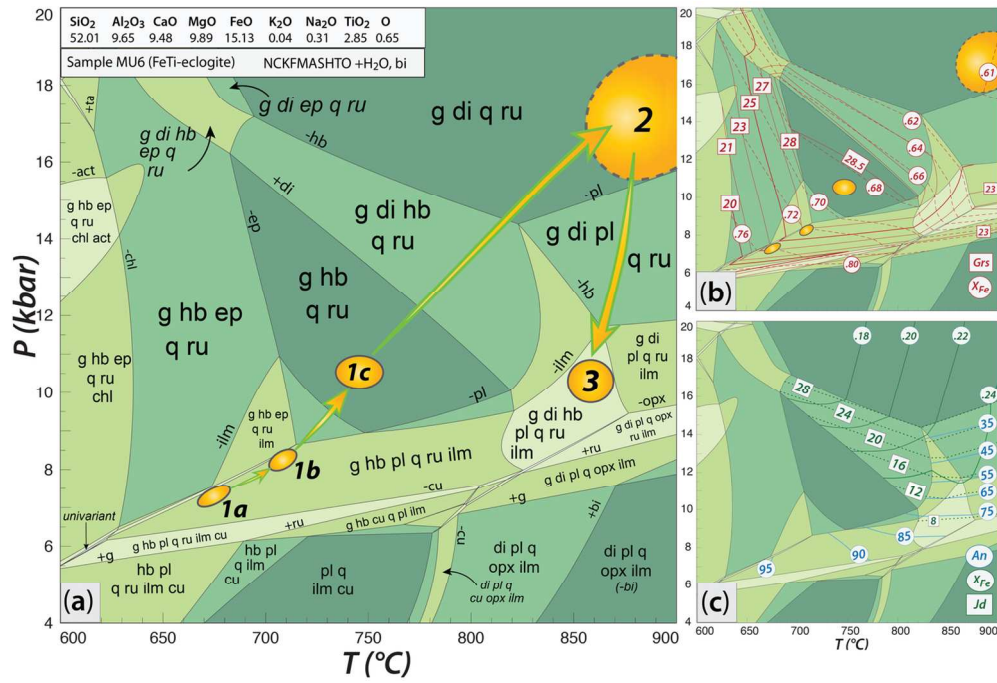


Figure 11: Pseudosection calculated for the Fe-Ti-rich eclogite (MU6). – 170mm
129x88mm (300 x 300 DPI)

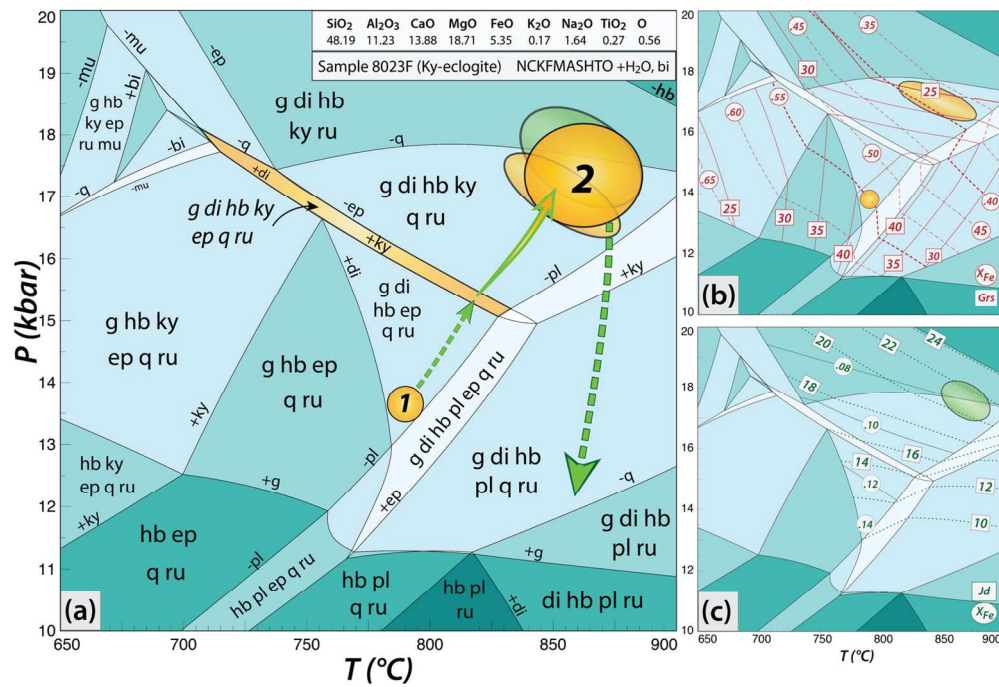


Figure 12: Pseudosection calculated for the kyanite eclogite (8023F). – 170mm

130x90mm (300 x 300 DPI)

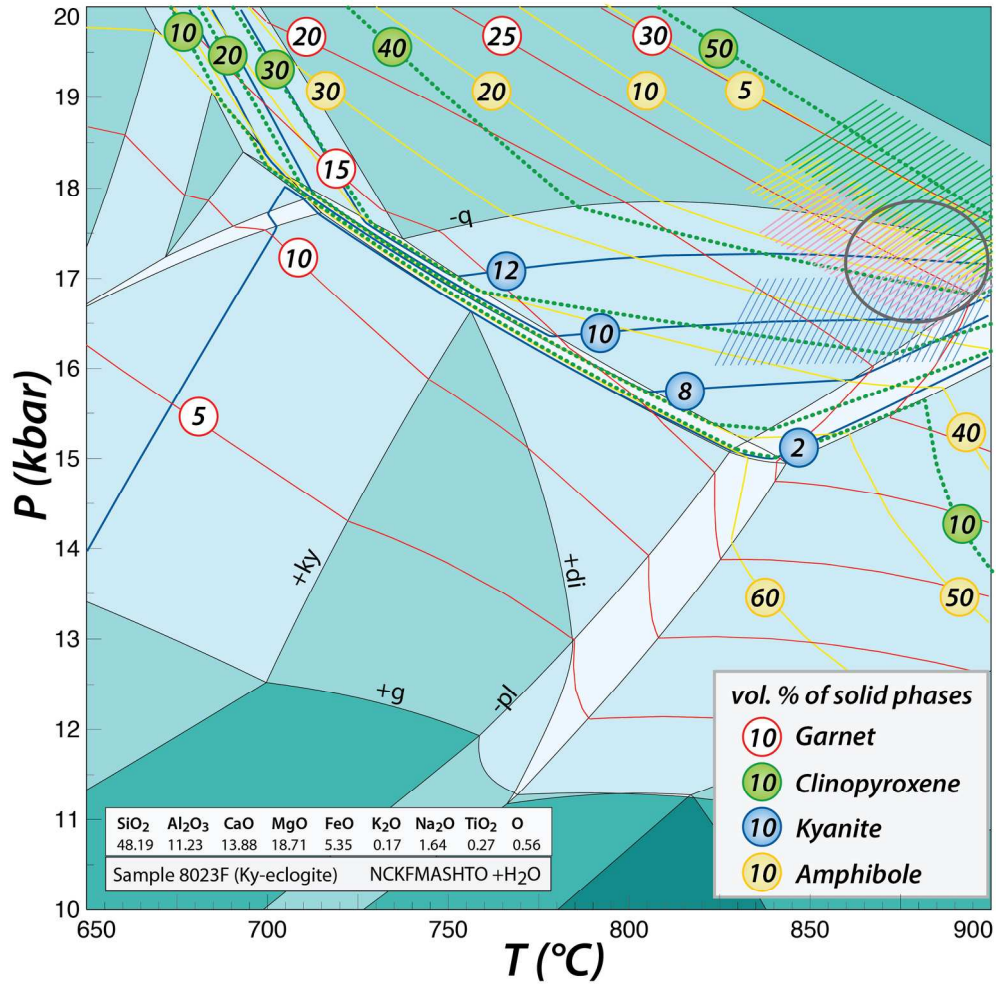


Figure 13: Pseudosection calculated for the kyanite eclogite (8023F; same as Figure 12) showing modal proportions of the major minerals in volume %. - 80mm

178x176mm (300 x 300 DPI)

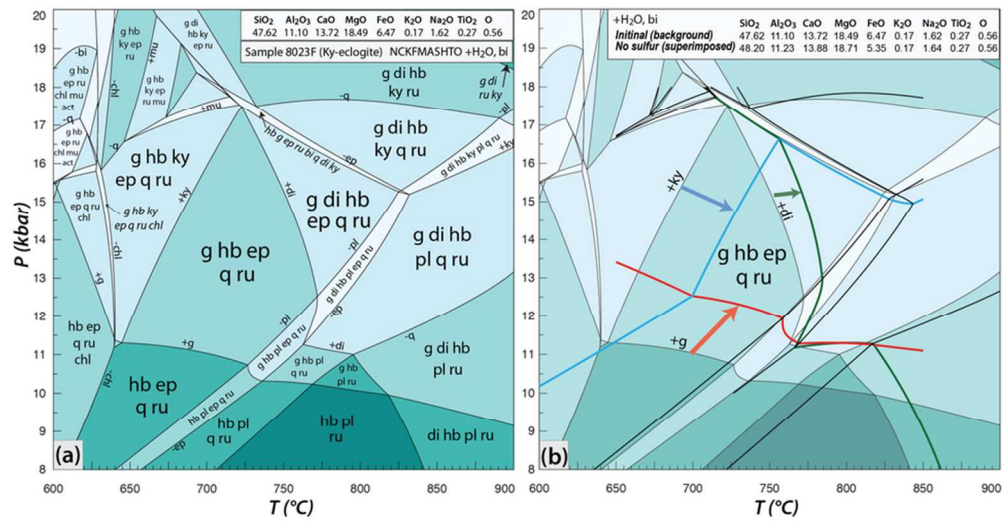


Figure 14: Effect of Fe²⁺ fractionation due to the presence of sulphides in the kyanite eclogite sample 8023F. – 170mm

82x42mm (300 x 300 DPI)

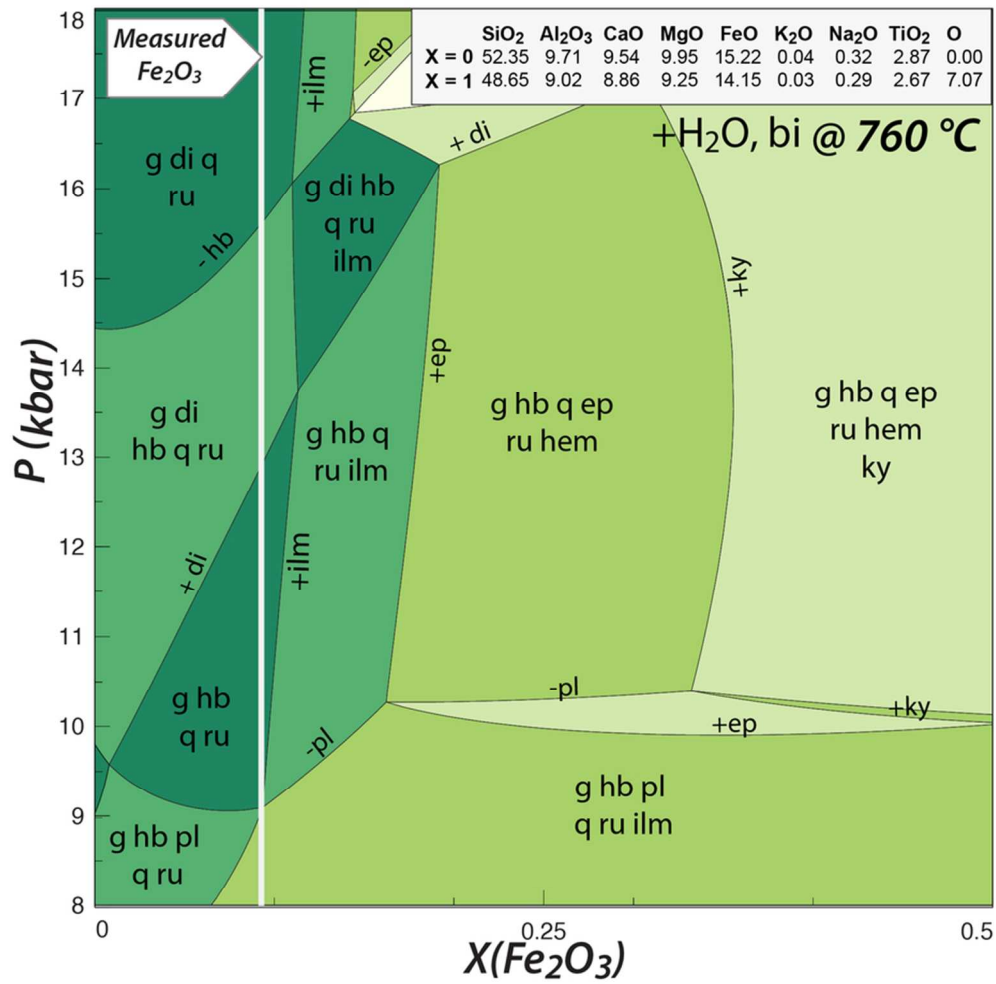
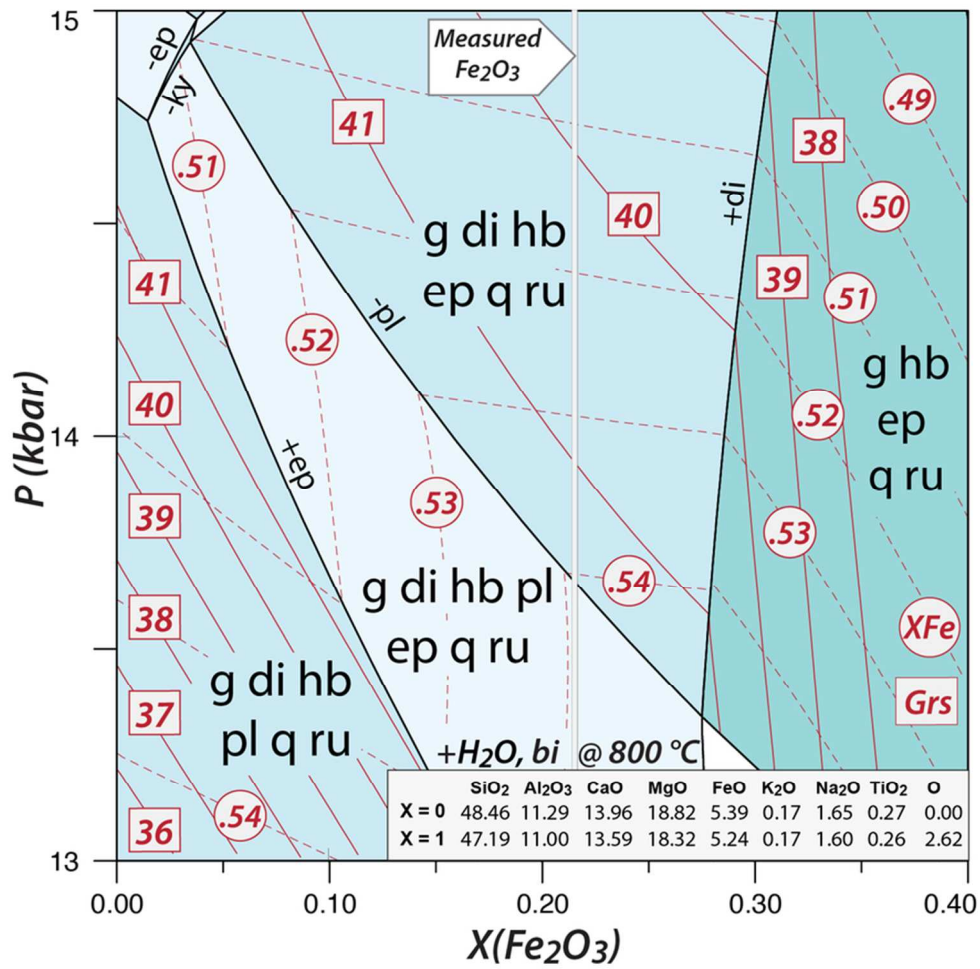


Figure 15: P-X(Fe₂O₃) pseudosection / Fe-Ti-rich eclogite sample MU6. – 80mm

79x78mm (300 x 300 DPI)

Figure 16: P-X(Fe₂O₃) pseudosection / kyanite-eclogite sample 8023F. – 80mm

76x74mm (300 x 300 DPI)

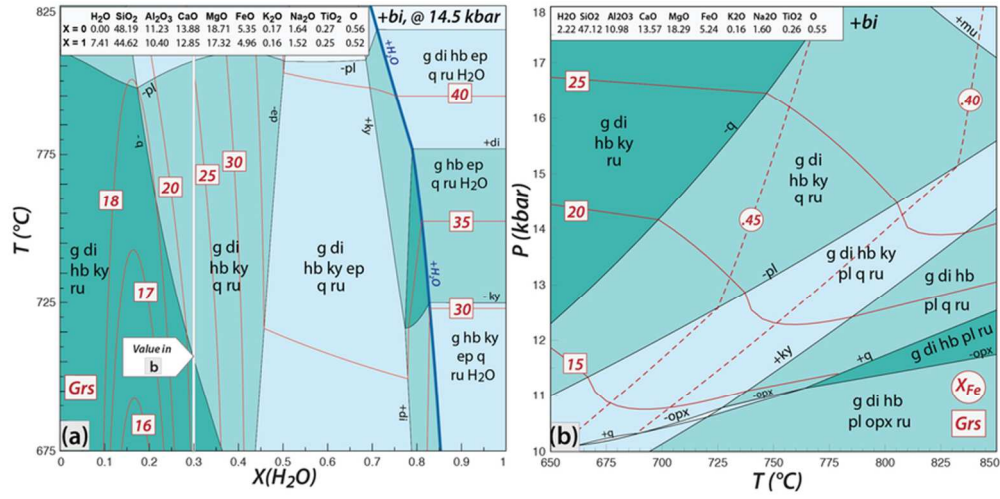


Figure 17: Effect of H₂O on the pseudosection of the kyanite-eclogite sample 8023F. – 170mm
78x38mm (300 x 300 DPI)

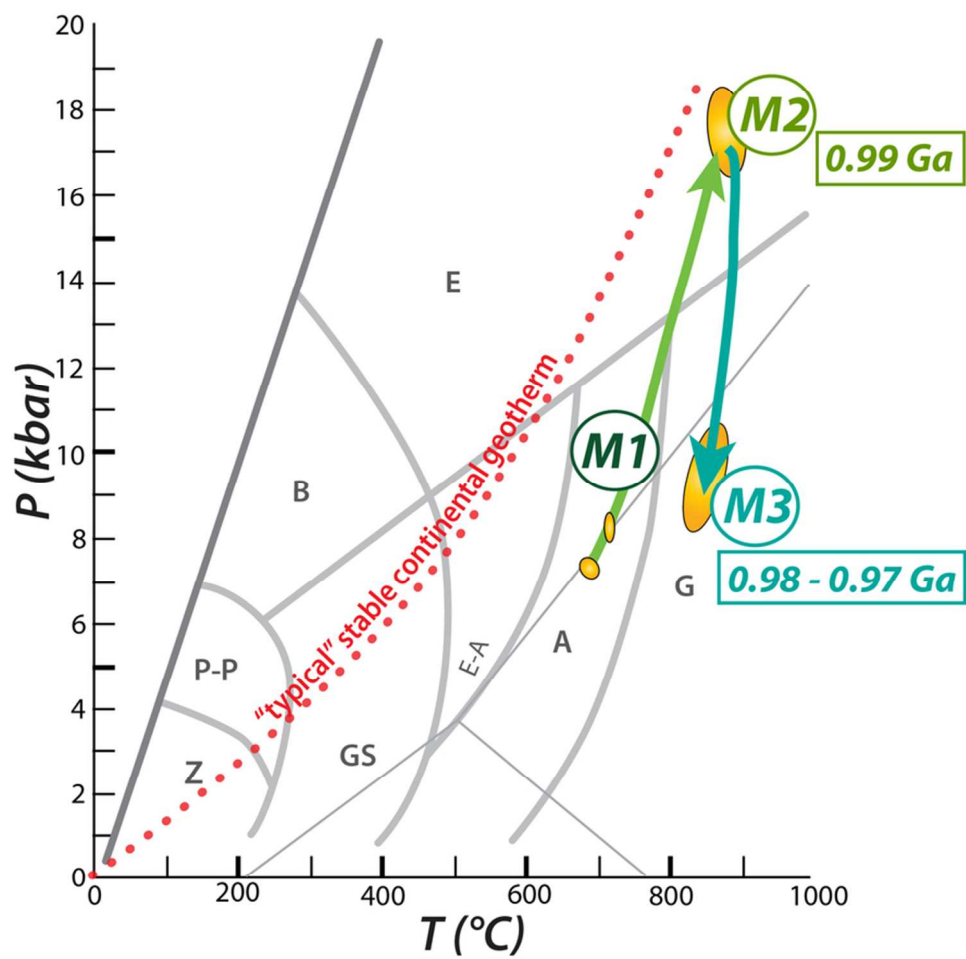


Figure 18: P-T path for Sveconorwegian eclogite, based on the modelling presented in this study. – 80mm

77x76mm (300 x 300 DPI)

Table 1a

Mineral	g	g	g	g	g	g	cpx	cpx	cpx	cpx	cpx	cpx
Sample	MU6	MU6	MU6	MU6	MU6	MU6	MU6	MU6	MU6	MU6	MU6	MU6
Name	6p245	6p251	6p225	6p270	6p205	6p299	6i3	6i4	6a123	6a215	6a208	6acp3
Location	core	core	outer core	outer core	rim	rim	inc g rim	inc g rim	mat	mat	mat	reint.
SiO ₂	37.87	37.59	37.75	38.14	38.46	38.89	51.32	51.57	48.69	49.94	50.57	53.17
TiO ₂	0.09	0.05	0.30	0.08	0.04	0.04	0.36	0.33	0.82	0.52	0.45	0.33
Al ₂ O ₃	20.62	20.76	21.20	21.39	21.72	22.03	4.02	3.64	6.21	5.89	5.51	11.4
Cr ₂ O ₃	0.00	0.00	0.00	0.07	0.00	0.03	0.00	0.00	0.03	0.00	0.00	0.06
FeO*	25.51	26.58	25.84	26.04	23.33	22.88	7.34	7.07	9.56	8.30	8.78	6.42
MgO	4.30	4.39	4.98	5.11	7.40	7.58	13.62	13.94	13.55	12.67	12.38	8.73
MnO	1.45	1.55	0.98	1.07	0.19	0.26	0.06	0.01	0.03	0.05	0.03	0.00
CaO	8.99	8.76	9.08	9.03	8.91	8.89	23.13	23.21	20.28	22.01	22.24	17.63
Na ₂ O	0.07	0.02	0.02	0.02	0.03	0.02	0.90	0.85	0.87	0.81	0.89	2.24
K ₂ O	0.05	0.01	0.01	0.00	0.00	0.00	0.01	0.01	0.07	0.01	0.02	0.10
Sum	98.96	99.71	100.14	100.96	100.09	100.62	100.76	100.63	100.10	100.21	100.86	100.08
Oxygens	12	12	12	12	12	12	6	6	6	6	6	6
Si	3.00	2.96	2.94	2.95	2.95	2.96	1.88	1.89	1.80	1.84	1.86	1.96
Ti	0.01	0.00	0.02	0.01	0.00	0.00	0.01	0.01	0.02	0.01	0.01	0.01
Al	1.92	1.93	1.95	1.95	1.96	1.98	0.17	0.16	0.27	0.26	0.14	0.49
Cr	0.00	0.00	0.00	0.00	0.00	0.00	0.00	0.00	0.00	0.00	0.00	0.00
Fe ²⁺	1.60	1.60	1.55	1.54	1.35	1.36	0.11	0.10	0.14	0.17	0.19	0.20
Fe ³⁺	0.09	0.15	0.13	0.14	0.15	0.10	0.12	0.11	0.15	0.08	0.08	0.00
Mg	0.51	0.52	0.58	0.59	0.85	0.86	0.74	0.76	0.75	0.70	0.68	0.48
Mn	0.10	0.10	0.07	0.07	0.01	0.02	0.00	0.00	0.00	0.00	0.00	0.00
Ca	0.76	0.74	0.76	0.75	0.73	0.73	0.91	0.91	0.80	0.87	0.88	0.70
Na	0.01	0.00	0.00	0.00	0.01	0.00	0.06	0.06	0.06	0.06	0.06	0.16
K	0.01	0.00	0.00	0.00	0.00	0.00	0.00	0.00	0.00	0.00	0.00	0.00
Sum	8.00	8.00	8.00	8.00	8.00	8.00	4.00	4.00	4.00	4.00	4.00	4.00
X _{Fe}	0.76	0.76	0.73	0.72	0.62	0.61	X _{Fe}	0.13	0.12	0.16	0.20	0.22
X _{Alm}	0.54	0.54	0.53	0.52	0.46	0.46						
X _{Prp}	0.17	0.17	0.20	0.20	0.29	0.29	X _{Id}	0.04	0.03	0.03	0.04	0.04
X _{Grs}	0.26	0.25	0.26	0.25	0.25	0.25						
X _{SpS}	0.03	0.03	0.02	0.02	0.00	0.01	X _{CaTs}	0.06	0.06	0.09	0.09	0.03

(* Total Fe oxide as FeO)

Table 1b

Mineral	pl	pl	pl	pl	am	am
Sample	MU6	MU6	MU6	MU6	MU6	MU6
Name	6i25	6i26	6a110	6a121	6a124	6i34
Location	inc g core	inc g core	xp. cpx corxp. cpx core		inc cpx core	inc g
SiO ₂	47.76	48.22	55.26	54.43	42.26	42.47
TiO ₂	0.00	0.00	0.00	0.01	2.03	1.82
Al ₂ O ₃	33.47	32.99	28.48	27.98	10.86	14.02
Cr ₂ O ₃	0.01	0.00	0.00	0.01	0.00	0.02
FeO*	0.25	0.25	0.27	0.15	13.21	12.17
MgO	0.00	0.00	0.00	0.00	13.41	13.05
MnO	0.02	0.00	0.00	0.00	0.04	0.03
CaO	17.03	16.31	10.94	10.43	11.75	12.27
Na ₂ O	2.18	2.57	5.79	6.04	1.52	1.77
K ₂ O	0.04	0.01	0.03	0.04	0.17	0.47
Sum	100.76	100.35	100.77	99.09	95.25	98.09
Oxygens	8	8	8	8	23	23
Si	2.18	2.21	2.48	2.48	6.30	6.15
Ti	0.00	0.00	0.00	0.00	0.23	0.20
Al	1.80	1.78	1.51	1.50	1.91	2.40
Cr	0.00	0.00	0.00	0.00	0.00	0.00
Fe ²⁺	0.01	0.01	0.01	0.01	0.94	1.06
Fe ³⁺	0.00	0.00	0.00	0.00	0.71	0.42
Mg	0.00	0.00	0.00	0.00	2.98	2.82
Mn	0.00	0.00	0.00	0.00	0.01	0.00
Ca	0.83	0.80	0.53	0.51	1.88	1.91
Na	0.19	0.23	0.50	0.53	0.44	0.50
K	0.00	0.00	0.00	0.00	0.03	0.09
OH					2.00	2.00
Sum	5.02	5.02	5.02	5.04	17.65	17.68
XAn	0.81	0.78	0.51	0.49	X _{Fe}	0.24
XAb	0.19	0.22	0.49	0.51	X _{Na_Mg}	0.03
XOr	0.00	0.00	0.00	0.00	(Na+K) _A	0.40

(* Total Fe oxide as FeO)

Table 1c

Mineral	g	g	g	g	g	g	cpx	cpx	cpx	cpx	cpx	cpx	cpx
Sample	8023F	8023F	8023F	8023F	8023F	8023F	8023F	8023F	8023F	8023F	8023F	8023F	8023F
Name	2pF446	2pF443	2pF422	2pF414	2pF404	2pF469	8Faird13	8Faird14	8pF913	8pF920	8pF937	8pF956	3pF118
Location	core	core	out_core	in_rim	rim	rim	inc_g	inc_g	core	out_core	out_rim	rim	rim
SiO ₂	39.34	39.01	39.29	38.74	39.52	40.01	51.10	50.59	52.41	52.78	52.38	52.75	52.41
TiO ₂	0.05	0.05	0.05	0.00	0.04	0.00	0.26	0.24	0.29	0.27	0.23	0.24	0.30
Al ₂ O ₃	21.95	22.12	22.1	22.21	22.22	22.79	7.78	8.00	7.83	7.94	7.53	7.50	8.00
Cr ₂ O ₃	0.07	0.04	0.04	0.03	0.10	0.07	0.02	0.07	0.04	0.08	0.08	0.05	0.07
FeO*	20.12	19.95	19.25	18.51	15.98	15.60	4.87	4.31	2.76	2.86	2.81	2.97	3.74
MgO	18.67	18.23	17.19	15.35	13.65	13.36	13.94	12.69	12.51	12.48	12.44	13.02	12.91
MnO	1.86	1.84	1.37	1.13	0.36	0.18	0.08	0.02	0.01	0.02	0.00	0.01	0.03
CaO	8.00	8.19	8.59	8.73	8.59	8.44	19.8	21.7	19.59	19.63	19.62	21.02	20.84
Na ₂ O	0.01	0.02	0.02	0.03	0.04	0.02	1.33	1.48	2.91	2.98	2.98	2.16	2.29
K ₂ O	0.01	0.00	0.01	0.00	0.00	0.02	0.00	0.01	0.02	0.01	0.01	0.01	0.01
Sum	100.50	100.19	100.45	99.77	99.24	100.23	99.66	99.14	98.37	99.06	98.08	99.75	100.58
Oxygens	12	12	12	12	12	12	6	6	6	6	6	6	6
Si	2.97	2.96	2.95	2.92	2.95	2.94	1.87	1.86	1.91	1.92	1.92	1.91	1.88
Ti	0.00	0.00	0.00	0.00	0.00	0.00	0.01	0.01	0.01	0.01	0.01	0.01	0.01
Al	1.96	1.98	1.96	1.97	1.95	1.98	0.34	0.35	0.34	0.34	0.33	0.32	0.34
Cr	0.00	0.00	0.00	0.00	0.01	0.00	0.00	0.00	0.00	0.00	0.00	0.00	0.00
Fe ²⁺	1.18	1.16	1.08	0.97	0.85	0.82	0.15	0.1	0.06	0.06	0.05	0.09	0.08
Fe ³⁺	0.09	0.11	0.13	0.20	0.15	0.14	0.01	0.03	0.02	0.02	0.03	0.00	0.03
Mg	1.02	1.01	1.09	1.16	1.38	1.44	0.76	0.69	0.68	0.67	0.68	0.70	0.69
Mn	0.12	0.12	0.09	0.07	0.02	0.01	0.00	0.00	0.00	0.00	0.00	0.00	0.00
Ca	0.65	0.67	0.69	0.70	0.69	0.67	0.77	0.85	0.77	0.76	0.77	0.82	0.80
Na	0.00	0.00	0.00	0.01	0.01	0.00	0.09	0.11	0.21	0.21	0.21	0.15	0.16
K	0.00	0.00	0.00	0.00	0.00	0.00	0.00	0.00	0.00	0.00	0.00	0.00	0.00
Sum	8.00	8.00	8.00	8.00	8.00	8.00	4.00	4.00	4.00	4.00	4.00	4.00	4.00
X _{Fe}	0.54	0.53	0.50	0.45	0.38	0.36	X _{Fe}	0.16	0.13	0.08	0.09	0.07	0.11
X _{Alm}	0.4	0.39	0.37	0.33	0.29	0.28							
X _{Pp}	0.34	0.34	0.37	0.4	0.47	0.49	X _{Id}	0.11	0.11	0.21	0.22	0.22	0.16
X _{Grs}	0.22	0.23	0.23	0.24	0.23	0.23							
X _{Sps}	0.04	0.04	0.03	0.02	0.01	0.00	X _{CaTs}	0.11	0.09	0.04	0.04	0.03	0.08

(* Total Fe oxide as FeO)

Table 1d

Mineral	spx		sp		sa		ss		bt		pl		pl		pl		pl		cp		cp		am		am								
Sample	802F	802F	802F	802F	802F	802F	802F	802F	802F	802F	802F	802F	802F	802F	802F	802F	802F	802F	802F	802F	802F	802F	802F	802F	802F	802F							
Name	8F817	8F8461	8F8443	8F8176	8F8445	8F8212			8F8170	8F8181	8F824	8F8242	8F8228	8F8229	8F8435	8F8111	8F8402			8F8535	8F819												
Location	cpx core		cpx core		sy close ru		sy close g		sy		grt core		sy close g		sy close ky		exp cpx		exp cpx		sy g		c opx		inc g		inc g		inc g		inc/oxp cpx		
SiO ₂	54.37	54.35	0.02	11.71	10.68	36.28			54.38	46.38	62.7	57.73	45.95	45.21	45.82	39.1	39.55			42.38	45.03												
TiO ₂	0.09	0.04	0.07	0.06	0.07	0.73			0.00	0.00	0.00	0.01	0.00	0.00	0.12	0.04	0.03			0.23	0.57												
Al ₂ O ₃	2.69	1.64	61.06	66.11	67.12	19.62			29.43	34.54	23.00	26.09	34.38	35.13	34.62	32.51	32.21			16.90	15.04												
Cr ₂ O ₃	0.07	0.12	4.27	0.20	0.69	0.00			0.00	0.02	0.02	0.00	0.01	0.00	0.02	0.01	0.01			0.00	0.17												
FeO*	13.13	14.23	20.27	5.42	5.55	8.75			0.21	0.14	0.07	0.11	0.13	0.11	0.15	1.86	1.98			5.45	4.85												
MgO	29.26	29.68	14.38	16.75	16.03	18.39			0.00	0.01	0.01	0.00	0.00	0.07	0.08	0.07	0.06			16.22	15.82												
MnO/Mn ²⁺	0.09	0.09	0.08	0.02	0.00	0.04			0.00	0.00	0.00	0.02	0.03	0.02	0.00	0.07	0.10			0.06	0.00												
CaO	0.19	0.30	0.03	0.19	0.08	0.05			11.76	17.87	4.96	8.46	18.16	18.71	17.91	24.72	24.61			11.78	12.12												
Na ₂ O	0.02	0.01	0.04	0.01	0.00	0.12			5.31	1.62	8.98	7.22	1.45	0.99	1.53	0.01	0.02			2.79	2.82												
K ₂ O	0.00	0.01	0.00	0.00	0.01	10.5			0.05	0.04	0.31	0.12	0.00	0.03	0.65	0.00	0.00			0.55	0.02												
Sum	99.94	100.49	100.21	100.48	100.23	94.54			101.14	100.61	100.04	99.77	100.11	100.26	100.31	98.41	98.57			96.45	96.51												
Oxygens	6	6	4	20	20	10			8	8	8	8	8	8	8	12	12			23	23												
Si	1.93	1.92	0.00	0.69	0.63	2.66			2.43	2.12	2.78	2.60	2.12	2.08	2.11	2.97	2.99			6.08	6.43												
Ti	0.00	0.00	0.00	0.00	0.00	0.04			0.00	0.00	0.00	0.00	0.00	0.00	0.00	0.00	0.00			0.03	0.06												
Al	0.11	0.07	1.89	4.56	4.65	1.70			1.55	1.86	1.20	1.38	1.87	1.91	1.88	2.91	2.87			2.86	2.53												
Cr	0.00	0.00	0.09	0.01	0.03	0.00			0.00	0.00	0.00	0.00	0.00	0.00	0.00	0.00	0.00			0.00	0.02												
Fe ²⁺	0.37	0.34	0.43	0.21	0.22	0.54			0.01	0.01	0.00	0.00	0.01	0.00	0.01					0.37	0.58												
Fe ³⁺	0.02	0.08	0.02	0.06	0.05	0.00			0.00	0.00	0.00	0.00	0.00	0.00	0.00	0.12	0.13			0.29	0.00												
Mg	1.55	1.57	0.56	1.46	1.41	2.01			0.00	0.00	0.00	0.00	0.00	0.01	0.01	0.01	0.01			3.47	3.37												
Mn/Mn ²⁺	0.00	0.00	0.00	0.00	0.00	0.00			0.00	0.00	0.00	0.00	0.00	0.00	0.00	0.01	0.01			0.01	0.00												
Ca	0.01	0.01	0.00	0.01	0.01	0.00			0.56	0.88	0.24	0.41	0.9	0.92	0.88	2.01	2.00			1.81	1.85												
Na	0.00	0.00	0.00	0.00	0.00	0.02			0.46	0.14	0.77	0.63	0.13	0.09	0.14	0.00	0.00			0.78	0.78												
K	0.00	0.00	0.00	0.00	0.00	0.98			0.00	0.00	0.02	0.01	0.00	0.00	0.00	0.00	0.00			0.10	0.00												
OH						2.00									1.00	1.00				2.00	2.00												
Sum	4.00	4.00	3.00	7.00	7.00	9.95			5.02	5.02	5.01	5.03	5.02	5.01	5.02	9.02	9.01			17.77	17.63												
Y _{Fe}	0.19	0.18	0.43	0.13	0.14	0.21	XAn		0.55	0.86	0.23	0.39	0.87	0.91	0.86					X _{Fe}	0.10	0.15											
XAb							XAb		0.45	0.14	0.75	0.60	0.13	0.09	0.13					X _{Na}	0.66	0.68											
XO _{Fe}							XO _{Fe}		0.00	0.00	0.02	0.01	0.00	0.00	0.00					(Na+K) _{Fe}	0.77	0.62											

(* Total Fe oxide as FeO)

Table 2

Sample	SiO ₂	Al ₂ O ₃	Fe ₂ O ₃ *	FeO	MgO	CaO	Na ₂ O	K ₂ O	TiO ₂	P ₂ O ₅	MnO	Cr ₂ O ₃	Sum
MU6	46.99	14.99	18.06	14.86	5.96	8.75	0.29	0.05	3.41	0.61	0.29	0.01	99.66
8023F	45.81	18.22	8.24	6.14	11.89	12.34	1.60	0.25	0.34	0.05	0.17	0.10	99.83

* = Total Fe oxides

P-T evolution of Precambrian eclogite, Sveconorwegian orogen, SW Sweden.

Lorraine Tual¹, Pavel Pitra^{2,3}, Charlotte Möller¹

¹ Geologiska institutionen, Lunds universitet, Sölvegatan 12, SE-223 62 Lund, Sweden.

lorraine.tual@gmail.com

² Géosciences Rennes, UMR CNRS 6118, Université Rennes 1, 35042 Rennes, Cedex, France

³ Česká geologická služba, Klárov 3, 118 21, Praha 1, Czech Republic

SUPPORTING INFORMATION

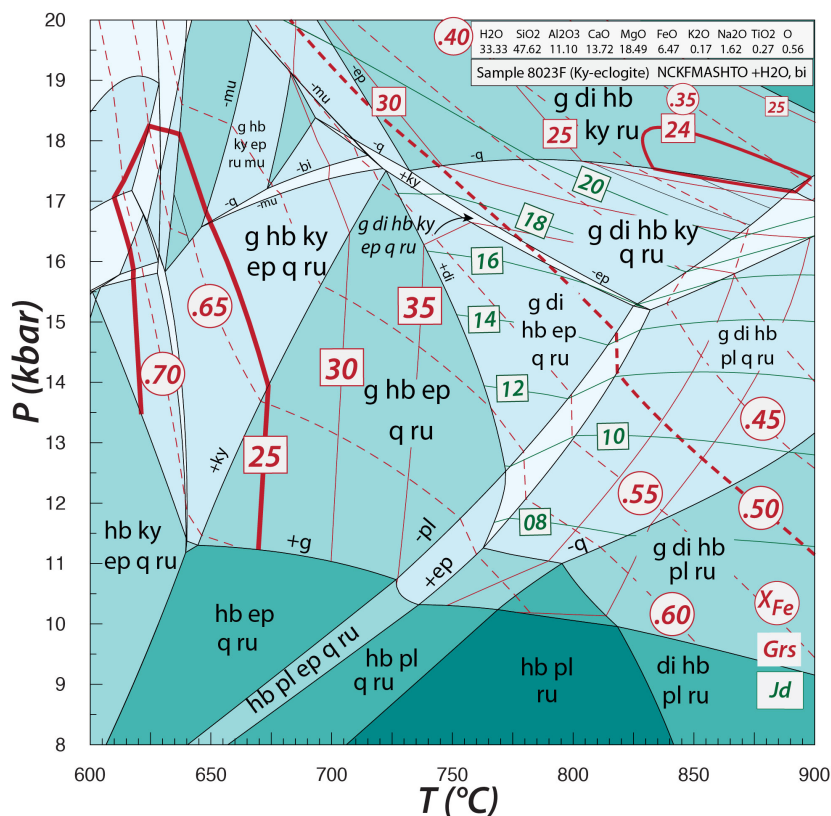


Figure S1:

Pseudosection calculated for the kyanite eclogite (8023F), ignoring Fe fractionation in sulphide. The rock composition is given as mole-% oxide. Compositional isopleths for garnet and clinopyroxene are shown in red and green, respectively.

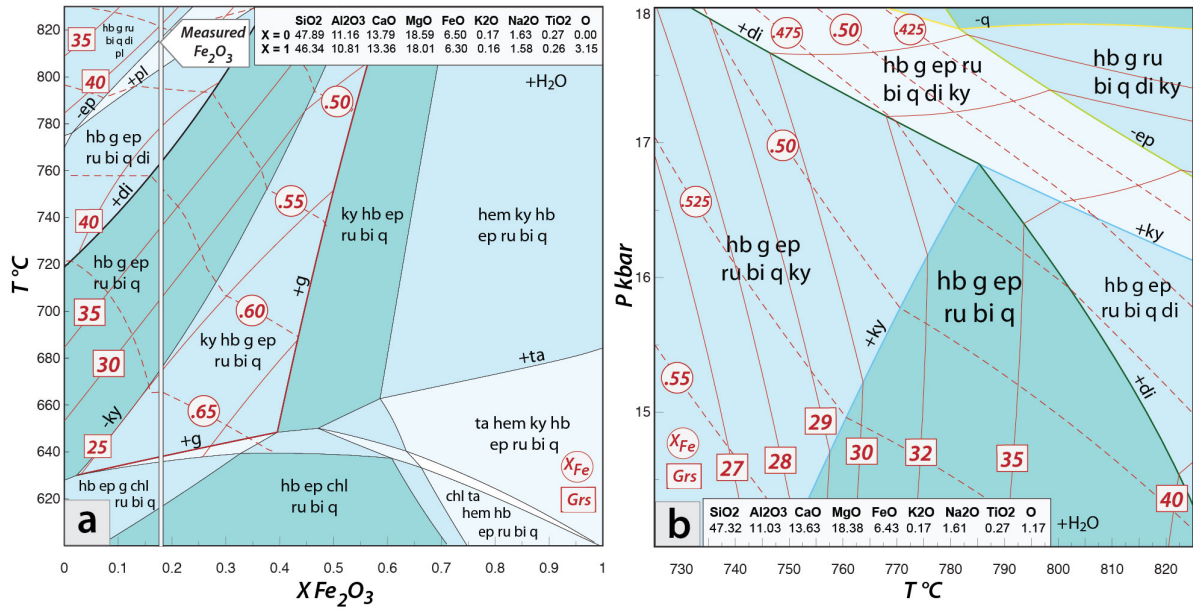


Figure S2:

T-X(Fe_2O_3) pseudosection showing the effect of Fe_2O_3 (a) on the paragenesis at 14 kbar, between 610 and 830 °C, for the kyanite-eclogite sample 8023F – Fractionation of Fe in sulphide is not considered. The bulk rock compositions in mole-% oxide corresponding to minimum and maximum possible amount of Fe_2O_3 ($X = 0$ and $X = 1$, respectively) are given in the upper right. The pseudosection is calculated in the range of $X = 0$ and $X = 1$. The white line marks the Fe_2O_3 value corresponding to the measured Fe_2O_3 . (b) P-T pseudosection showing the effect of increasing Fe_2O_3 , using a value corresponding to $X = 0.37$ in (a).